WANL-PR-(DD)-014
November 1, 1966

Westinghouse Astronuclear Laboratory

ANALYTICAL INVESTIGATION OF TURBINE EROSION PHENOMENA

Interim Technical Report Number 1, Volume 1
Contract NAS 7-390

WANL-PR-(DD)-014
November 1, 1966

Westinghouse Astronuclear Laboratory

ANALYTICAL INVESTIGATION OF TURBINE EROSION PHENOMENA

Interim Technical Report Number I, Volume I

Contract NAS7-390

INFORMATION CATEGORY

Unclassified

D. M. Haughey 10/28/66

AUTHORIZED CLASSIFIER DATE

PREFACE

This report describes the construction and application of an analytical model of turbine rotor blade erosion in wet vapor turbines as performed under Contract NAS 7-390. The model is used to estimate erosion values for the analytical simulations of a nine-stage wet vapor steam turbine and a two-stage wet vapor potassium turbine. Comparison of operating results from the actual turbines with the calculated values gives a substantial degree of quantitative agreement. While the present degree of quantitative agreement may in part be fortuitous, the model selected appears to be adequate for at least order of magnitude turbine erosion estimation and provides an excellent base for refinement. This is the first of an intended series of technical reports. It is expected that later reports in this series will add substantial refinement to the model and provide more detail as to solutions to the equations of the model.

This report is divided into three volumes. Volume I is an account of the overall model with a rather extensive summary of the many component processes which contribute to the model. Volume II describes in more detail the fluid,dynamic and thermodynamic processes of the model. Volume III discusses an examination of the influence of the external variables on the rates of erosion of turbine blade materials under repetitive impact of liquid drops and chemical dissolution in flowing liquid.

ACKNOWLEDGEMENTS

Messrs. F. J. Heymann and L. G. Hays have provided much useful information through their contacts at various laboratories in Great Britain: Messrs. J. L. Eaton, D. Pearson, D. G. Christie and many others. Additional acknowledgement is given to the useful discussions and guidance provided by Mr. Hays in his capacity as NASA Program Manager on Contract NAS7-390.

In connection with the form, staffing, and general approach to carrying out this project, many thanks are due Mr. C. E. Sinclair for his useful suggestions, advice and helpful actions. Similar thanks are due Mr. E. Murphy with respect to the procedural and monetary aspects of the Contract.

Thanks are also due Mr. F. K. Fischer, Steam Division and Dr. W. A. Stewart, Research Labs, for the loan of the very knowledgeable personnel who made the construction of this analytical model of turbine blade erosion a possibility.

Acknowledgement is also due Mr. B. G. Rieck and his staff for editing and publishing the report volumes.

Astronuclear Laboratory

VOLUME I

ASSEMBLY OF ANALYTICAL MODEL OF WET VAPOR TURBINE BLADE EROSION

Authors:

W. D. Pouchot, R. E. Kothman, W. R. Fentress, F. J. Heyman,
J. D. Milton, F. R. Arcella

TABLE OF CONTENTS

Section		Page
PREFACE		I-iii
ACKNOWLEDGEMENTS		I-iv
PART A:	INTRODUCTION	I-1
PART B:	ANALYTIC MODEL OF EROSION IN WET VAPOR TURBINES	I-2
1.0	GENERAL PROCESS	I-2
2.0	TURBINES EXAMINED	I-6
2.1	Yankee Atomic Plant Low Pressure Turbine	I-6
2.2	Two-Stage Potassium Turbine	I-10
3.0	DETAIL PROCESS	I-13
3.1	Condensation, Nucleation and Growth	I-13
3.2	Vapor Boundary Layer Flow and Wakes	I-25
3.3	Deposition of Moisture on the Surface of the Blades	I-29
3.4	Movement of Moisture on Blade Surfaces	I-38
3.5	Atomization and Trajectories of Damaging Liquid	I-40
3.6	Material Removal	I-52
4.0	CALCULATED EROSION RATES	I-58
4.1	Yankee Turbine	I-58
4.2	Discussion of Results	I-62
4.3	Two-Stage Potassium Turbine	I-65
PART C:	CONCLUSIONS AND RECOMMENDATIONS	I-68
REFERENCES		I-70

LIST OF ILLUSTRATIONS

Figure		Page
B-1	Relation of Moisture Particle Travel to Motion in Plane Normal to Axis of Rotation	I-4
B-2	Impingement on Rotating Blade	I-5
B-3	Schematic of Yankee Turbine	I-8a
B-4	Yankee Steam Turbine	I-9
B-5	Erosion, Last Rotating Row--Yankee Turbine	I-11
B-6	Second Rotor; Two-Stage Potassium Test Turbine	I-14
B-7	Moisture Fraction in Divergent Portion of Nozzle	I-18
B-8	Droplet Growth in Divergent Portion of Nozzle	I-19
B-9	Results of Blade Wake Calculation for Ninth Stator Blade at 3/4 Height Position, Yankee Turbine	I-28
B-10	Wake Pressure Side Velocities, Ninth Yankee Stator	I-30
B-11	Collection Efficiency, Ninth Stage Stator Nose Yankee Turbine	I-32
B-12	Portion Collected, Ninth Stage Stator Nose Yankee Turbine	I-33
B-13	Two-Stage Potassium Turbine	I-34
B-14	Portion of Drops Collected, Concave Side Ninth Stator Yankee Turbine	I-36
B-15	Portion of Drops Collected, Concave Side Two-Stage Potassium Turbine	I-37
B-16	Ninth Yankee Stator, Primary Atomization, Average Drop Diameter	I-43
B-17	Primary Atomization Distribution, Ninth Stator Yankee Turbine	I-45
B-18a	Ninth Yankee Stator Wake, Weber Number versus Distance at Y/Yo - 0.01 Suction Side	I-46

Figure		Page
B-18b	Ninth Yankee Stator Wake,Weber Number versus Distance at Y/Yo - 0.01 Pressure Side	I-47
B-19	Impacting Drop Size Distribution, Critical Weber Number = 22;Ninth Yankee Rotor Pressure Side Wake of Stator Calculation	I-49
B-20	Yankee Turbine Ninth Rotor, Drop Impact Velocities	I-50
B-21	Axial Length Impingement Zone (Maximum)	I-51
B-22	Stellite Erosion Rates--Data from Pearson	I-57
B-23	Correlation of Data of Person by Use of "Critical Velocity"	I-59

LIST OF TABLES

Table		Page
B-1	Major Steps in Erosion Calculation	1-7
B-2	Yankee Steam Turbine, Row by Row Mean Diameter Data	1-8b
B-3	Potassium Turbine, Row by Row Mean Diameter Data	1-12
B-4	Comparison of Condensation - Performance Program Results with Equilibrium Expansion at Mean Diameter for the Yankee Turbine	1-20
B-5	Mean Droplet Diameter Based on Equilibrium Moisture and Number of Drops Obtained from Condensation Performance Program for Yankee Turbine	1-22
B-6	Comparison of Condensation and Equilibrium Performance Calculation for Potassium Turbine	1-23
B-7	Moisture and Drop Size Distribution at Exit from First Stage Rotor of Potassium Turbine	1-24
B-8	Calculated Boundary Layer Properties, Yankee Turbine	1-26
B-9	Yankee Steam Turbine, Ninth Stator Liquid Flow	1-40
B-10	Solution - Rate Constants	1-54
B-11	Calculated Erosion Ninth Rotor Yankee Turbine Maximum Stable Drop Size Criterion - $W_e = 22$, Pressure Side Wake	1-63
B-12	Calculated Erosion Ninth Rotor Yankee Turbine Maximum Stable Drop Size Criterion - $W_e = 22$, Suction Side Wake	1-63

PART A

INTRODUCTION

The objective of this study reported herein is to provide an analytical-empirical model of turbine erosion which fits and explains experience in both steam and metal vapor turbines. Because of the complexities involved in analyzing turbine erosion problems, in a pure scientific sense it was obvious that this goal could be only partially realized. Therefore, emphasis was placed on providing a useful model for preliminary erosion estimates for given configurations, fluids, and flow conditions. In terms of the prescribed effort level, this goal was given precedence over the more interesting but less immediately fruitful goal of precise and comprehensive mathematical definition of the processes contributing to erosion.

This first volume of this study describes the assembly of the overall model of erosion, summarizes the component process models used and describes the application of the model to a nine-stage wet vapor steam turbine and a two-stage wet vapor potassium turbine. The model is used to estimate erosion depths on the rotor blades of the turbines examined and the results are compared to operating experience.

The qualitative aspects of the model follow, to a large extent, opinions on the erosion process in wet vapor steam turbines that are widely held within the steam turbine community at the present time. In respect to the quantitative aspects, the study is indebted to excellent previous studies by Gyarmathy[1] and Gardner[2]. It is a refinement and extension of these two previous works (more the former than the latter) based on later experience and substantial additional component process theory and computation.

While an effort has been made to make this report sufficient in itself to provide calculational understanding of the erosion model and its components, because of the complexities of some of these processes, knowledge of the referenced material may be required for a comprehensive understanding.

PART B

ANALYTIC MODEL OF EROSION IN WET VAPOR TURBINES

1.0 GENERAL PROCESS

The model outlined here is concerned with the erosion of the nose and leading edge of rotor blades of turbines operated in wet vapor. While other regions of erosion have been observed, the chief area of erosion in turbines of well ordered flow operated at or near their design conditions, is on the inlet edge of the rotor blades.

As the vapor expands in a wet vapor turbine the temperature of the vapor is reduced below the saturation point until supersaturation becomes sufficient to cause spontaneous condensation.* The thermodynamic condition at initiation of rapid spontaneous condensation is called the Wilson line, and its location is a function of the particular vapor properties and the rate at which the vapor is expanding. For a vapor such as steam or potassium the location of the Wilson line generally corresponds to a degree of supersaturation equivalent to an equilibrium moisture content of less than 4.5%. At the Wilson line condensation takes place rapidly, and the moisture content quickly approaches equilibrium. Thereafter, (in the turbines examined) the expansion process follows with but slight lag an equilibrium expansion.

The original spontaneous nucleation creates sufficient surface area to allow further condensation to occur with minimal supersaturation. As originally formed, the condensation nuclei are extremely small (.01 μ diameter) and are of relatively uniform size because of the short time period involved. The nuclei grow quite rapidly to about 0.2μ diameter as the supersaturation potential created by the expansion in advance of spontaneous condensation is exhausted. Thereafter a slower growth takes place as the droplets progress through the turbine. The final size attained may approach 1μ in diameter.

---

* Calculations by Gyarmathy [1] show that compared to spontaneous condensation the other processes of condensation are of negligible importance in a wet vapor steam turbine. We are assuming this to be true for liquid metal vapor turbines on the basis that the casings could be thermally insulated if necessary to make it true.

Because of their small size, the condensate particles are essentially locked to the vapor flow and most of them remain with the stream tube of their birth until turbine exit*. However, a small percentage of the condensate fog collects on surfaces because of the curvature of the flow passages and rotation of the moving blades. By calculation, the percentage collected per turbine row even in the wettest rows is of the order of 5% or less of the total fog present; generally it is less**. The collected moisture causes the erosion. The fog particles cause no erosion since they follow the vapor flow as it slices cleanly over the blading surfaces.

The small percentage of fog particles collected form into rivelets, films, and drops on the blading surfaces. On the rotating blading the predominant force is that of the centrifugal field of the blades. Under this force, the liquid collected on the rotors flows nearly radially outwards and is thrown from the tips of the blades. The particle flow, illustrated in figure B-1, is essentially in the tangential direction and the initial flow velocity is approximately the same as the peripheral speed of the blade. The tangential distance of travel in large turbines is often in the order of 5 inches.

Due to the high peripheral velocity of the turbine blade tips, the liquid flung from the tips is well atomized. However, it is still large in size compared to the fog particles. Most of these atomized drops proceed in an almost undisturbed trajectory to impact the turbine casing at a very shallow angle. Even with a 5-inch path length the time of flight is less than 0.5 millisecond at 1200 ft/sec tip velocity. This time is too short for the vapor drag forces to produce any appreciable deceleration or acceleration of most of the flung liquid. A small percentage of the liquid is undoubtedly in the form of small drops (of sufficiently high surface to mass ratio) that are turned into the succeeding stator by the vapor stream. However, such drops will slice cleanly along the stators and cause no damage. For these

---

* Normal secondary flows at hub and tip and will modify this picture somewhat. There is also a negligible drift of the particles relative to the vapor in a radial direction due to the turbine centrifugal field. Calculated average radial drift velocity, Yankee Turbine - 0.12 ft/sec.

** This calculation is in qualitative agreement with the observation that moisture removal devices in central station type steam turbines rarely remove as much as 25% of the total moisture present even though moisture is removed at a number of spots lengthwise along the turbine.

reasons erosion at the inlet of stators* is seldom encountered in practice where the moisture impinging on the casing is removed through suitable slots**. For the same reasons the assumption is made in the model, as applied to the Yankee turbine, that there is negligible collected liquid carryover from rotor row to stator row.

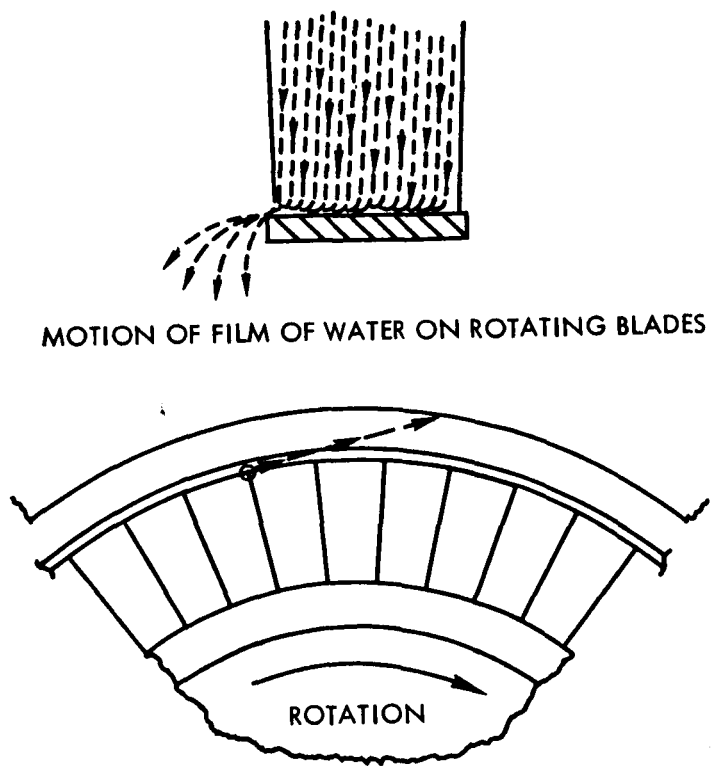

Figure B-1. Relation of Moisture Particle Travel to Motion in Plane Normal to Axis of Rotation

---

* Erosion at the exit of stators is sometimes observed and assumed to be caused by drops rebounding from the rotor blades.

** Some vapor flow into these slots is required to keep drops rebounding from the casing from rejoining the main stream flow.

On the stator blades, the primary force acting on the collected liquid is the drag force of the mainstream flow. Under this force the liquid flows to the rear of the stator where it collects until torn from the stator as rather large particles. In the model used it is assumed that the collected liquid follows the bulk flow streamlines and on a time average basis is uniformly distributed along a stator from hub to tip. Although the first assumption is of doubtful validity because of the secondary flows at blade hub and tip,* the second assumption is still reasonable, since the liquid displaced from the pressure surface of a particular stator will flow over the casing or rotor hub and terminate on the suction surface of a companion stator.

The liquid which is torn from the back of stator vanes causes the erosion that this model seeks to explain in a quantitative manner. Most of the large liquid drops torn from the stators undergo further breakup and all undergo acceleration between stator and rotor. However, in the time available they attain only a fraction of vapor stream velocity, and because of the vector velocity difference, the drops strike the nose and convex surfaces of the rotating blades (figure B-2). Due to the high velocity of the liquid drops relative to the rotor blades, some of

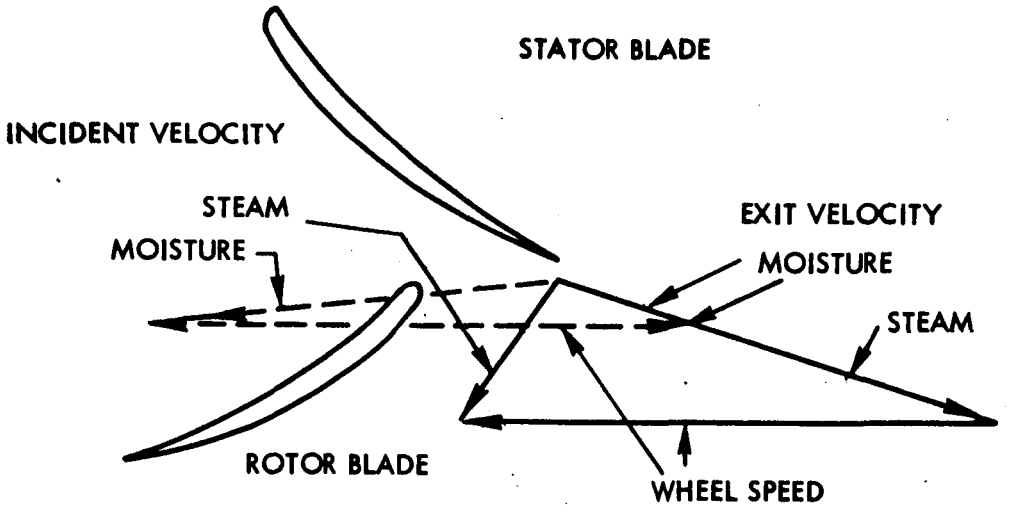

Figure B-2. Impingement on Rotating Blade 611131-89B

* There is an added force on the liquid on the stators tending to move it from tip to hub in the form of the turbine radial pressure gradient. This force is considered to be of negligible importance. Average ratio of radial velocity to axial velocity calculated for Yankee Turbine 9th stator - .003.

the larger drops strike with sufficient intensity to cause material removal by repetitive impact*. The erosion of the rotor blades is confined to the nose and leading edge of the convex surface because of shadow effect of companion blades. Because the blade speed is highest at the tip and hence the incident drop velocities are highest, the greatest degree of erosion occurs at the blade tips.

As can be inferred from the preceding remarks the impact intensity and degree of erosion depend in large part on the extent to which the large drops are accelerated and atomized after being torn from the trailing edge of the stationary blades. In this respect, pressure is an important parameter. For example, in high pressure turbines large particles are more completely atomized and accelerated and there is less erosion than in low pressure turbines. Axial spacing between the stator and rotor blade row also affects erosion rate since the spacing influences the distance of travel, residence time, and the amount of acceleration. The importance of atomization and acceleration also places a premium on good clean fluid dynamic design in wet vapor turbines as an important tool in reducing erosion.

On the basis of this verbal description of a turbine blade erosion model, the kinds of fluid-dynamic, thermodynamic, and strength of materials calculations which are required can be outlined in a general way. Such a general outline of the calculations is provided in Table B-1.

2.0 TURBINES EXAMINED

2.1 Yankee Atomic Plant Low Pressure Turbine (Figure B-3)

The steam turbine for the example calculations is the low-pressure turbine of a tandem compound steam turbine. This turbine is used in the Yankee atomic power plant.

The reasons for selecting this particular turbine are threefold: the blade erosion has been observed for an approximate period of 5 years, the exhaust moisture content is high, and the expansion is entirely below the saturation line. The latter feature is similar to that postulated for alkali metal space power systems.

---

* Some of the large drops torn initially from the stators are caught in the low velocity wake of the stator blades and do not break up further prior to rotor blade impact. Most of the initial drops are completely reatomized to smaller particles before impact and cause relatively little damage.

MAJOR STEPS IN EROSION CALCULATION

INPUT

Geometric, Fluidynamic, Thermodynamic

Turbine inlet and exit state and operating rpm.
Detail turbine flow path geometry.
Working fluid thermodynamic and physical properties.
Estimate of polytropic efficiency, flow coefficients, seal leakage for each turbine row.

Calculations

Establish flow areas of each turbine row as a function of axial length. (Herein, area variation versus length was approximated by an equation as the calculational techniques used made it desirable.)

Calculate bulk flow state conditions (vapor pressure, temperature, quality velocities) at mean diameter before and after each row, assuming the vapor remains in thermodynamic equilibrium.

Condensation

Using mean diameter blade speeds, blade angles and flow area, solve equations of energy, continuity, momentum and condensation stepwise with length through successive blade rows. Calculate and record bulk flow state conditions, condensate particle radii, number, distribution of sizes, mean radius of particles until condensate particle areas become sufficient to sustain near equilibrium condensation of potential moisture.
(See Volume I, Section B-3.1)

After near-phase equilibrium has been established, discontinue use of condensation equation. Calculate and record average condensate particle size at inlet and exit of each subsequent turbine row on basis of average growth required of number of particles present to maintain equilibrium.
(See Volume I, Section B-3.1)

Check condensate formation by condensation on turbine casing. If competitive with bulk condensation, adjust model of Volume I Section B-3.1) to include effects and continue. (Effect is not included in present model and is probably unimportant in most turbines.)

Condensate Particle Collection

Assuming inertial impaction means by which condensate collects, calculate amount of condensate collected at each row based on bulk flow conditions at 3/4 blade height condition for stages where possibility of erosion is suspected.
(See Volume I, Section B-3.3)

Estimate amount of collected moisture carried over from previous stages. If small compared to particular stage collection, ignore (as was done here). If large, adjust collected moisture for carryover and continue.

Bulk Flow Fluidynamics

Maintaining thermodynamic equilibrium assumption, expand mean diameter calculations to obtain bulk flow state conditions at exit and entrance of blade rows from hub to tip. Satisfy conditions of simplified radial equilibrium of flow as a minimum.

Select stages where possibility of erosion is suspected. Calculate and record blade surface velocities at 3/4 blade height position through stator blades of these rows.
(See Volume I, Section B-3.2)

Boundary Layer and Wake Fluidynamics

Using blade surface velocities previously calculated, integrate Trunkenbrodt equation along blade section and pressure surfaces from nose to trailing edge to determine boundary layer conditions, particularly at blade trailing edge.
(See Volume I, Section B-3.2)

Using boundary layer velocity distributions at trailing edge of blades, estimate decay and spreading of wake downstream of trailing edge.
(See Volume I, Section B-3.2)

Check drift of condensate particles relative to vapor in radial direction as a result of turbine centrifugal flow field in blade rows. If large, adjust collection model for moisture concentration in the vapor towards the tips of blades. If small, ignore (as was done here).

Check drift of liquid film on stators in radial direction relative to vapor streamlines under impress of turbine radial pressure gradient. If large, adjust collection model to account for increased liquid concentration toward hub. If small, ignore (as was done here).

Atomization of Collected Condensate

Using estimated amounts of collected moisture at stator trailing edges and stator trailing edge boundary layer friction coefficient, determine if liquid film Reynolds Number is great enough to produce ripples in film. (See Volume I, Section B-3.4) If ripples are produced, use primary atomization model formulated here. (Volume I, Section B-3.5) If ripples are not produced, formulate new primary atomization model and continue.

Establish drop size distribution resulting from primary atomization (See Volume I, Section B-3.5)

Follow the trajectories of a representative sampling of primary drops along various wake streamlines from center to edge of stator blade trailing edge wake. Determine and record maximum secondary atomization drop diameters and dispersion of drop velocities at plane of rotor inlet as a function of drop diameter and wake streamline.
(See Volume I, Section B-3.5)

Check breakup time of representative primary drops. If breakup time of unstable primary drops is longer than traverse time between stator and rotor, adjust final distribution accordingly. If breakup time for nearly all unstable primary drops is shorter than traverse time, ignore effect (as was done here).
(See Volume I, Section B-3.5)

Estimate and record distribution of drop diameters resulting from primary and secondary atomization processes as they exist at the inlet plane to the rotor blades.
(See Volume I, Section B-3.5)

INPUT

Blade Material Erosion Properties

Obtain material removal rates indicative of the "second stage" of erosion of the blade material as a function of: (1) working fluid, (2) amount of fluid impinging as drops, (3) size of drops, and (4) impact velocity normal to impacted surface. If empirical information is available, continue. If empirical information on particular fluid-material combination is unavailable, formulate material removal model. See Volume III for background material which may be useful in the formulation of such a model.

Impact of Atomized Drops with Rotor

Extrapolate velocities relative to stator of various diameter drops at the plane of the rotor inlet from those calculated at the 3/4 blade height position to other blade height positions. Herein it was assumed that these velocities referred to the 3/4 blade height position were proportional to the square root of the bulk flow dynamic pressures at the stator blade trailing edge.

Convert drop velocities relative to stator exit to velocities relative to rotor blade nose. Record both total velocity and velocity component normal to surface of nose. (Somewhere on the nose radius these two velocities are identical. This should be the point of maximum impact erosion.) Estimate and record axial lengths (measured from leading edge of rotor blade) of zones of moisture impacts as a function of drop diameter and dispersion of velocity for a given drop diameter.
(See Volume I, Section B-3.5)

Combine: (1) average area of zones of moisture impact in terms of selected drop diameter classes, (2) total collected moisture and (3) average distribution of moisture collected as a function of drop diameters, to estimate average local rates of moisture impacting on the nose of the rotor blades as a function of the selected drop diameter classes.

OUTPUT - LOCAL EROSION RATES

Combine local rates of moisture impact for selected drop diameter classes and impact velocity normal to rotor blade surface with correlated material removal rate information to estimate and record local rates of blade material removal as a function of blade height position.
(See Volume I, Section 3.6 & 4.0)

Check removal of rotor blade nose material by chemical dissolution. (See Volume II, Section 3.6) If large, add to material removed by impact. If small, ignore (as was done here).

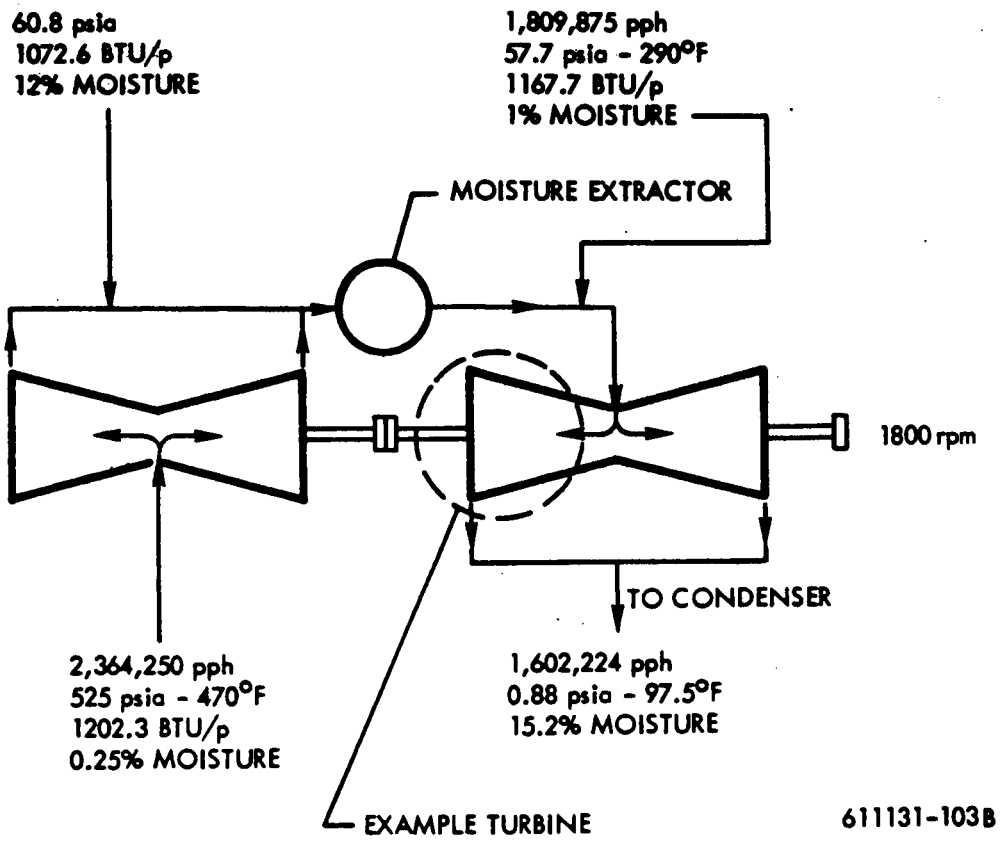

Figure B-3. Schematic of Yankee Turbine

Geometric and fluid dynamic data for design operation are given in table B-2. As shown, the moisture content varies from 1% at turbine inlet to about 15% at exit, the static pressure varies from 59.2 to 0.88 psia, the specific volume from 8.08 to 318.9 ft^3/lb, the maximum tip speed is 1238 ft/sec, the axial spacing varies from 0.5 in. at inlet to 1.9 in. at exit, and the trailing edge thickness is in the order of 0.055 to 0.075 in. at the exhaust end. Figure B-4 shows the example low-pressure turbine with blading cross sections for the 9th stator and rotor.

The turbine was placed in operation November 1960, and has operated since except for shutdowns in 1962 and 1964 for refueling the reactor.

At the time of the 1962 shutdown, after 18 months of operation, there was evidence of erosion on the leading edge of the rotor blades in the last blade row. While the intensity of the erosion varied throughout the row, the erosion position was roughly the same, extending an approximate distance of 2 in. from the tip of the blade with maximum intensity approximately

TABLE

Yankee Steam Turbine Ro

Row No.	9th Rotor	9th Stator	8th Rotor	8th Stator	7th Rotor	7th Stator	6th Rotor	6th S
Effective Blade Height, in.	40.00	37.44	27.23	24.46	21.01	19.47	15.07	14.0
Effective Mean Diameter, in.	117.50	118.40	110.64	109.41	106.01	104.78	100.13	98.5
Average Guaging	0.600	0.421	0.433	0.341	0.341	0.279	0.330	0.2
Exit Flow Angle, deg	37.0	25.0	25.6	20.0	20.0	16.2	19.2	16.9
Static Pressure, psia	0.88	1.515	2.313	3.411	5.072	6.573	8.745	10.6
Moisture Content	0.152	0.140	0.130	0.120	0.108	0.100	0.0911	0.0
Temperature, ^{o}F	97.5	115.9	131.5	146.5	162.8	174.1	187.0	196.4
Specific Volume, cfpp	318.9	194.5	131.9	92.6	64.7	51.19	39.59	33.0
Jet Velocity, fps	1133.	1057.	1016.	1026.	857.0	905.7	779.8	811.5
Mean Wheel Speed, fps**	922.8	929.9	869.0	859.3	832.6	823.0	786.4	773.9
Tip Wheel Speed, fps**	1237.0	1224.0	1082.8	1051.4	997.6	975.9	904.8	884.2
Inlet Flow Angle to Next Row, deg	90.0	86.27	83.92	73.32	95.34	79.52	97.74	89.6
Inlet Velocity to Next Row, deg	690.	456.	453.	378.	297.	266.	265.	242.
Blade Reynolds No. x 10^{-5} ***	1.5	5.9	2.2	7.9	3.4	8.2	5.7	6.1
Steam Flow, pph x 10^{-3}	801.1	801.1	801.1	801.1	801.1	801.1	801.1	801.1
Centrifugal Force, G's								
Mean Diameter	5400.							
Tip Diameter	7220.							
Axial Space Stator Exit to Rotor Inlet, in.	1.9		1.7		1.1		0.6	
Trailing Edge Thickness, in.	0.066	0.077	0.065	0.063	0.060	0.055	0.045	0.0
Blading Material	12% Chromium Steel							
Stellite Shields	yes		yes		yes		yes	

*Generally, values are for exit of blade row.

**Stator blade "wheel speed" is that speed equivalent to a rotor of the same diameter.

***Reynolds Number based on the blade chord and exit velocity.

1-86-1

ow Mean Diameter Data *

5th Rotor	5th Stator	4th Rotor	4th Stator	3rd Rotor	3rd Stator	2nd Rotor	2nd Stator	1st Rotor	1st Stator	Inlet
12.77	11.81	10.57	9.98	9.15	8.47	7.42	6.84	6.49	6.30	7.55
96.77	95.25	93.50	92.51	91.35	90.27	89.28	88.64	88.35	88.10	89.35
0.270	0.266	0.300	0.286	0.278	0.274	0.277	0.268	0.248	0.231	--
15.7	15.4	17.5	16.6	16.1	15.9	16.1	15.5	14.4	13.4	--
13.331	16.367	19.386	22.748	26.473	30.521	34.852	39.679	45.345	51.931	59.2
0.0768	0.0693	0.0630	0.0560	0.0500	0.0440	0.0380	0.0310	0.0240	0.0170	0.0100
207.1	217.5	226.3	234.9	243.2	251.3	259.0	266.8	274.9	283.4	292.0
27.11	22.56	19.39	16.81	14.68	12.93	11.50	10.25	9.11	8.08	--
800.0	744.2	727.3	709.7	700.6	686.5	692.7	699.0	705.4	689.1	--
760.0	748.1	734.4	726.6	717.5	709.0	701.2	696.2	693.9	692.0	--
860.3	840.8	817.9	805.0	789.3	775.5	759.5	749.9	744.9	741.4	--
87.36	98.72	100.5	103.1	103.1	104.8	100.94	97.2	93.7	97.8	90.0
222.	208.	224.	210.	202.	196.	198.	192.	180.	165.	--
7.6	6.4	5.3	6.3	5.2	11.6	8.4	8.2	9.5	14.7	--
801.1	801.1	904.9	904.9	904.9	904.9	904.9	904.9	904.9	904.9	904.9
								4050.		
0.5		0.5		0.5		0.5		0.5		
0.045	0.015	0.038	0.0125	0.037	0.010	0.038	0.010	0.033	0.010	
yes		yes		no		no		no		no

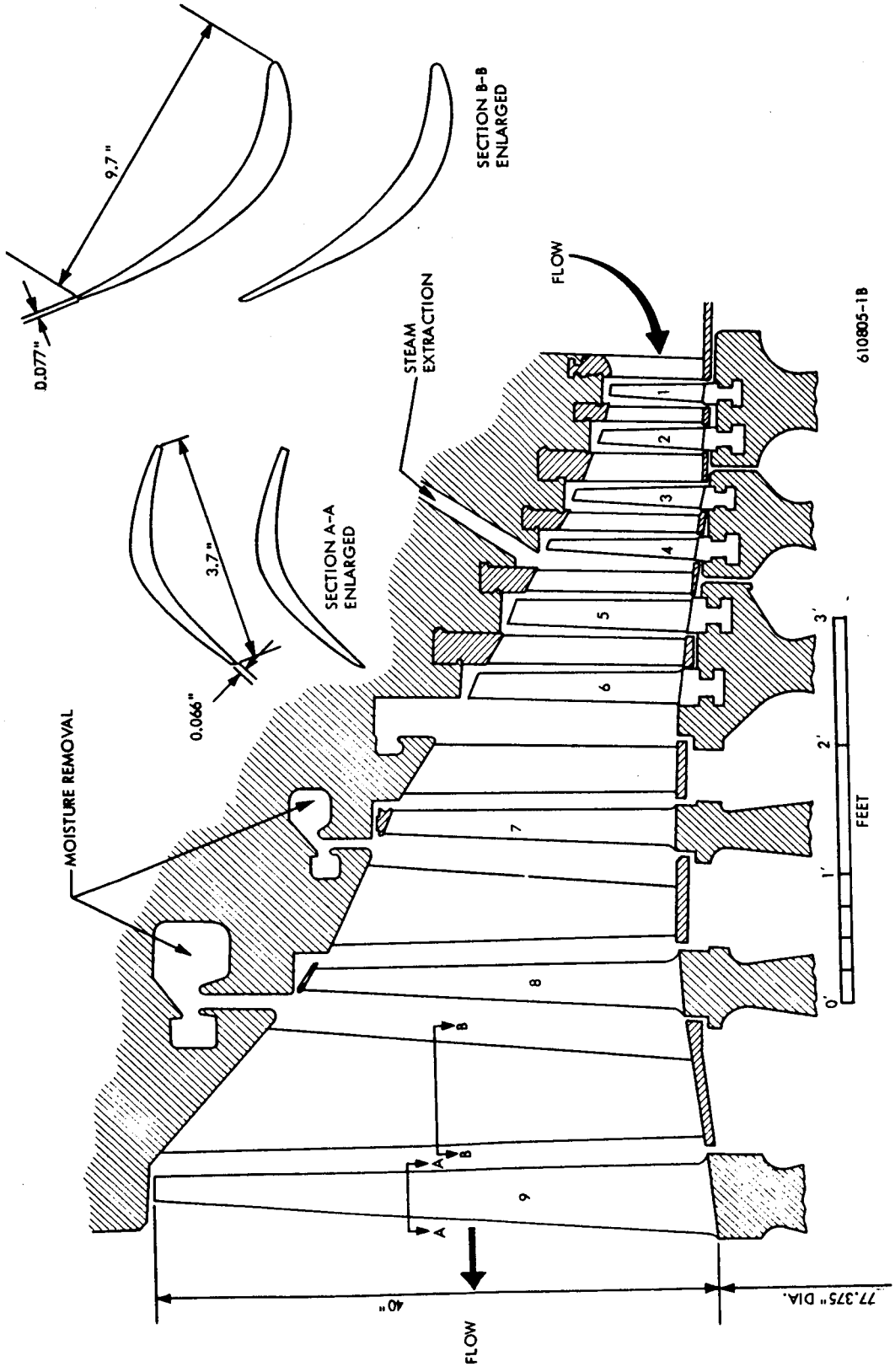

Figure B-4. Yankee Steam Turbine

3/4 in. from the tip. The depth of erosion varied from a maximum of 1/8 to 3/16 in. (about 8 blades) to a minimum of no more than a roughening of the inlet edge. Figure B-5 shows one of the worst of the 196 blades in this row; 15 Stellite shields were replaced, but none of the blades was replaced. Erosion in the 7th and 8th row was slight (no replacement of shields), nil in the first six blade rows, and nil in the stator blade rows. This condition was roughly the same in both ends of the double flow turbine.

Observations at the time of the 1964 shutdown were about the same, with the exception that the 7th row erosion had progressed slightly and the 8th stage erosion was, as before, practically nil. There is no satisfactory explanation for this anomaly. Again, the last stage erosion was roughly as before.

2.2 Two-Stage Potassium Turbine

The two-stage potassium test turbine of Contract NAS 5-1143 is, to our knowledge, the only multi-stage alkali metal vapor turbine of a space type which has been operated for a substantial length of time (some 2,000 hours). As such, it is an obvious choice as an example turbine in connection with the analytical investigation of turbine blade erosion. While the two-stage potassium test turbine was designed as the third and fourth stages of a five-stage turbine for a space Rankine power plant (4), it has actually operated as the first two stages of a turbine insofar as the inlet vapor quality is concerned.

The two-stage potassium turbine design described here approximates the test turbine design but is not identical*. The operating conditions (Reference 3) are:

Speed, 19,100 rpm	Flow, 2.64 pps
Inlet temperature, 1600°F	Inlet pressure, 38.2 psia
Inlet moisture content, 1%	Total to total pressure ratio, 2.95

Other fluid dynamic and geometric data are given in Table B-3**. As shown, the

*The two-stage potassium turbine design presented here was constructed on the basis of the readily available data on the G. E. two-stage potassium test turbine from Reference 4, 5, and 6. These references do not contain information on the stationary blading sections, the turbine seal arrangement and appear to be inconsistent with respect to stationary row gaging Therefore, the design as presented has Westinghouse stationary rows. It is not believed that this makes any important difference with respect to the erosion model discussion.

**Based on equilibrium calculations.

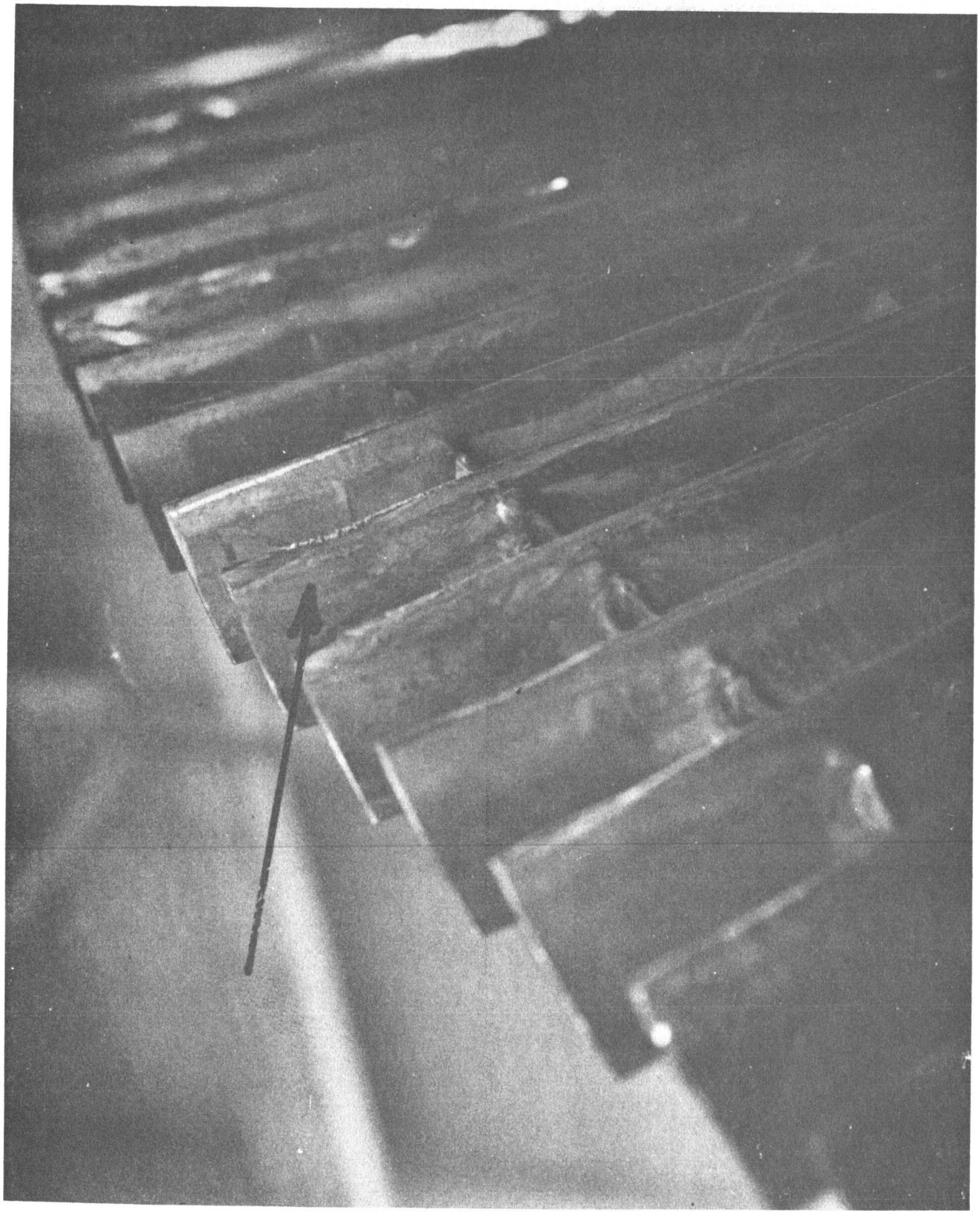

Figure B-5. Erosion, Last Rotating Row - Yankee Turbine

TABLE B-3

Potassium Turbine

Row by Row Mean Diameter Data*

	Inlet	1st Stator	1st Rotor	2nd Stator	2nd Rotor
Effective Blade Height, in.	0.595	0.745	0.761	0.992	0.937
Effective Mean Diameter, in.	7.575	8.078	8.120	8.677	8.713
Average Gaging	--	0.322	0.435	0.360	0.520
Exit Flow Angle, deg	--	18.75	25.8	21.1	31.45
Static Pressure, psia	38.2	28.03	22.6	15.92	11.9
Moisture Content	0.01	0.035	0.048	0.069	0.085
Temperature, ^{o}R	2060.	1987.	1940.	1869.	1811.
Specific Volume, cfpp	13.2	17.2	20.8	28.3	36.8
Jet Velocity, fps	--	1075.	939.	1105.	1041.
Mean Wheel Speed, fps**	--	673.	681.	724.	726.
Tip Wheel Speed, fps**	--	--	737.	--	805.
Incident Flow Angle to Next Row, deg		45.0	68.4	52.4	73.4
Incident Velocity to Next Row, fps	344.	490.	438.	503.	566.
Blade Reynolds No. x 10^{-5}***		3.86	1.81	2.78	1.38
Mass Flow, pps	2.64	2.64	2.64	2.64	2.64
Centrifugal Force, G's					
Mean Diameter	--	--	42100.	--	45200.
Tip Diameter	--	--	45900.	--	50000.
Axial Space, Stator Exit to Rotor Inlet, in.		0.2		0.2	

* Values are for exit of blade row unless otherwise indicated.

** Stator blade "wheel speed" is the equivalent speed for a rotor of the same diameter.

*** Reynolds No. based on the blade chord and exit velocity.

moisture content of the vapor varies from 1% at turbine inlet to 8 1/2% at exit, the static pressure varies from 38.2 to 11.9 psia, the vapor specific volume from 13.2 to 36.8 ft^3/lb, the maximum tip speed is 805 ft/sec, the trailing edge thickness of the blades is 0.015 in., the axial spacing between rows is 0.2 in. and the effective mean diameter of the last stage rotor blade (bucket) has an effective mean diameter of 8.71 in. with an effective height of 0.937 in.

The data presented in table B-3 is as though the expansion in the two-stage turbine were at equilibrium moisture content throughout the turbine. On the basis of the condensation calculations (Section 3.1) the expansion is that of a supersaturated vapor until near the exit of the first rotor. Comments on the differences may be found on page 1-21.

A portion of the General Electric two-stage potassium test turbine (Contract NAS 5-1143) is pictured in figure B-6.[37] This is the second stage rotor after 2,000 hours operation. As can be seen, there is little evidence of erosion.

3.0 DETAIL PROCESSES

The overall erosion model is composed of a number of component processes. They are discussed in the following sequence: (1) condensation, nucleation and growth, (2) boundary layer flow and wakes, (3) collection of moisture on blade surfaces, (4) movement of moisture on blade surfaces, (5) atomization of collected moisture and subsequent trajectories and (6) material removal.

3.1 Condensation, Nucleation and Growth

A large number of experimental and theoretical condensation studies have been reported and excellent reviews are given by Stever[7] and Courtney[8]. Condensation theory has been applied to condensing flow in nozzles by Oswatitish[9], Glassman[10] and others[11, 12]. The

Second Stage Turbine Wheel After
2000 Hour Endurance Test (Forward Face)

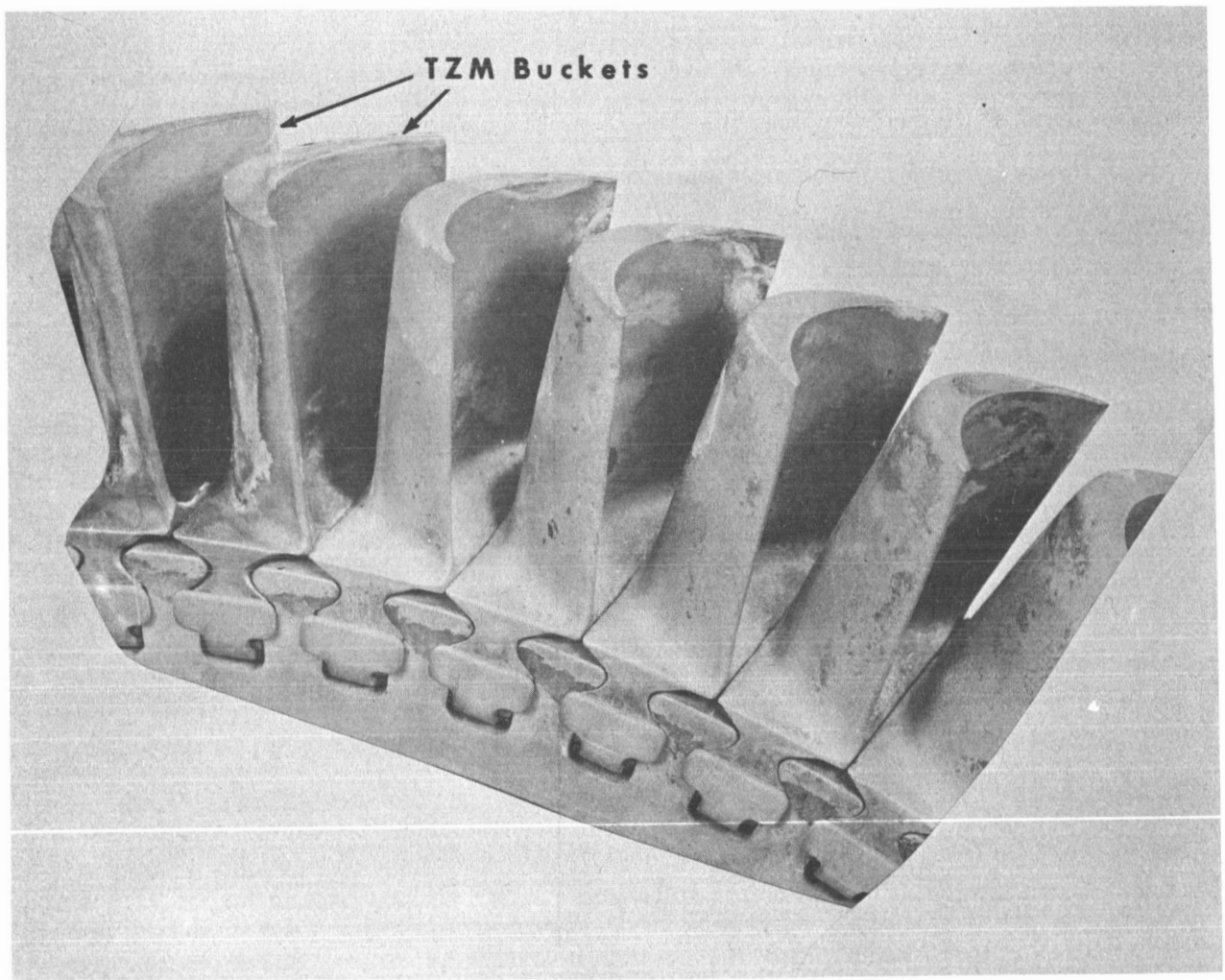

Figure B-6. Second Rotor, Two-Stage Potassium Test Turbine

present analysis follows the same general method of solution which was first described by Oswatitish[9] but uses improvements introduced by Gyarmathy[1] and others. There is good agreement between theoretical results and experiments conducted for water vapor. Experiments involving potassium vapor are inconclusive.[35]

The basic method used is to describe the condensing flow by the one-dimensional energy, momentum and continuity equations including the effects of condensation. The condensation process is described by the rate of formation of droplets and their rate of growth. The rate of formation of condensation nuclei in a supersaturated vapor is predicted by nucleation theory. Thermodynamic and heat transfer principles are then applied to predict rate of growth. The equations and the computer program written to perform the numerical calculations are discussed in Volume II.

Nucleation and Growth Theory

The concept of a critical drop size which is in thermodynamic equilibrium with a supersaturated vapor is fundamental to all nucleation theory. This critical radius is given by the Helmholtz equation. The equilibrium defined by this relation is metastable; smaller drops tend to evaporate, larger ones tend to grow by condensation. Where a vapor becomes supersaturated, to obtain the lowest energy state the vapor should condense, but condensation must start with the formation of small drops which are unstable. As supersaturation is increased, the critical size decreases and the likelihood of survival increases until at a certain supersaturation, appreciable condensation into a fog of droplets occurs. The rate at which these nuclei are formed is given by a rate equation of the Arrhenius type according to the classical steady state nucleation theory model taken. This classical theory is attributed to Frenkel[13].

Although many modifications of the classical theory have been derived to account more precisely for additional effects such as variation of surface tension with radius, the classical

equation is usually chosen to describe the nucleation rate. A time delay may be involved before the nucleation reaches its steady rate[14]. If the time constant were as large 10 μ sec, the location of the condensation point in the turbine would only be shifted several hundredths of an inch downstream. Thus, it is reasonable to neglect the transient nucleation effects. One of the most questioned limitations of nucleation theory involves surface tension. The accuracy of surface tension measurements for the liquid metals is uncertain due to the scatter in reported data. The second limitation concerns the application of the surface tension concept to small clusters of molecules. In some instances the critical nuclei contain only a few tens of molecules and it is difficult to visualize such a cluster as a spherical droplet having surface tension corresponding to a flat surface. However, examination of the stable size of charged colloidal particles in strong electrostatic fields indicates that the change in surface tension must be small to radii as low as 20 Å in lead or bismuth. [36]

Once the nuclei are formed, their growth rate is primarily governed by the rate at which the latent heat can be transferred from the drops to the surrounding vapor. The mode of heat transfer from the drop to the vapor may differ depending on existing conditions. The mean free path in the vapor is considerably larger than the critical sized nuclei so that during the early growth of drops heat transfer is by free molecular processes. As size increases, the process passes through the transition region and at large sizes normal gaseous conduction or convection occurs.

At the critical size the droplet temperature is equal to the vapor temperature. As the droplet grows, its temperature T_r must remain somewhat lower than the saturation temperature corresponding to the local pressure due to the effect of surface tension.

The subcooling due to the surface tension effect, termed "capillary supercooling" (by Gyarmathy), is equal to the product of the supercooling and the ratio of the critical radius to the droplet radius. Thus, the maximum temperature difference between the drop and the vapor is a function of radius. The assumption is that droplet growth is controlled solely by heat transfer limitations, and that there is an adequate number of molecular collisions

with the drop to supply growth. This would not be the case, for example, if water condensation in air were being considered. In that case, diffusion of water molecules through air to the droplet surface would be a definite factor limiting growth rate. With heat transfer controlling the growth rate, it is assumed that the drop always has the maximum temperature permitted by its radius.

Results for a Convergent-Divergent Nozzle

To check the one dimensional condensation performance computer code, a calculation was carried out in which steam was expanded in a convergent-divergent nozzle. Some of the results are shown in figures B-7 and B-8. Condensation does not occur until the divergent section is reached, so only the divergent portion is shown. The results agree with other authors' calculations.[12]

Condensation Results for Yankee Turbine

The computer program input data describing the Yankee turbine consisted of steam properties, turbine tip diameter, hub diameter, mean blade angles, blade spacing and blade thickness. The inlet steam was assumed to be supersaturated at 57.5 psia with 1% moisture equivalent.

The calculated values of pressure, temperature, axial velocity, and moisture at the exit of the blade rows are presented in table B-4. This table also shows mean diameter calculations which are based on the equilibrium expansion mode. The results are not directly comparable due to the small difference in inlet pressure. The results of the two methods compare very well, except in the first stator where the assumed inlet supersaturation affects the temperature. The calculations were terminated at the end of the third stage. At this point the flow nearly approached equilibrium with a supercooling of only 0.6°F. A hand calculation indicated that sufficient droplet surface area was available for subsequent condensation to proceed with negligible supercooling.

During the expansion, the steam remained supersaturated throughout the first stator. Condensation began in the first rotor. The Wilson point was reached at 70% of the axial distance through the first rotor and corresponded to 2.18% theoretical moisture. The total number

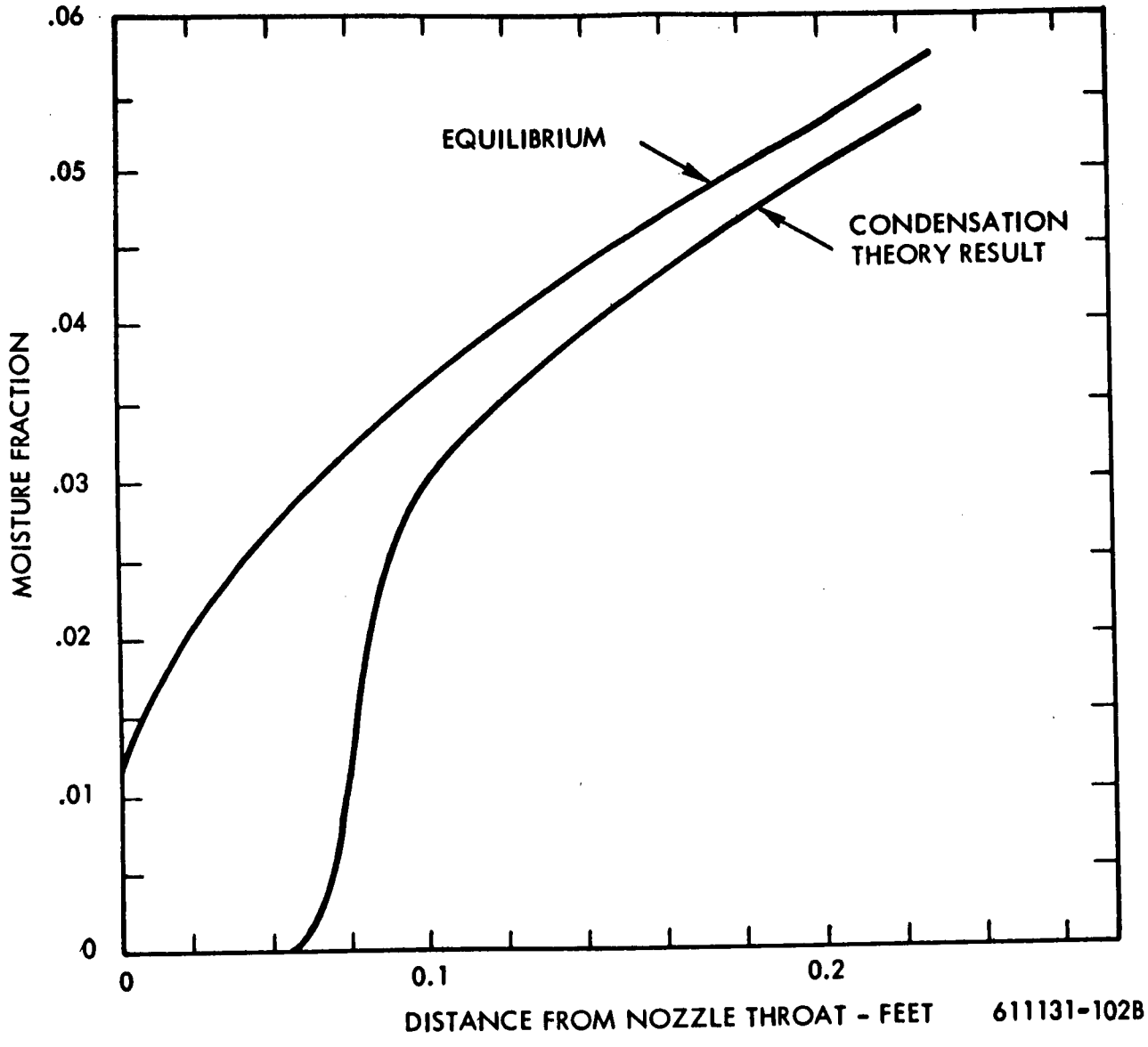

Figure B-7. Moisture Fraction in Divergent Portion of Nozzle

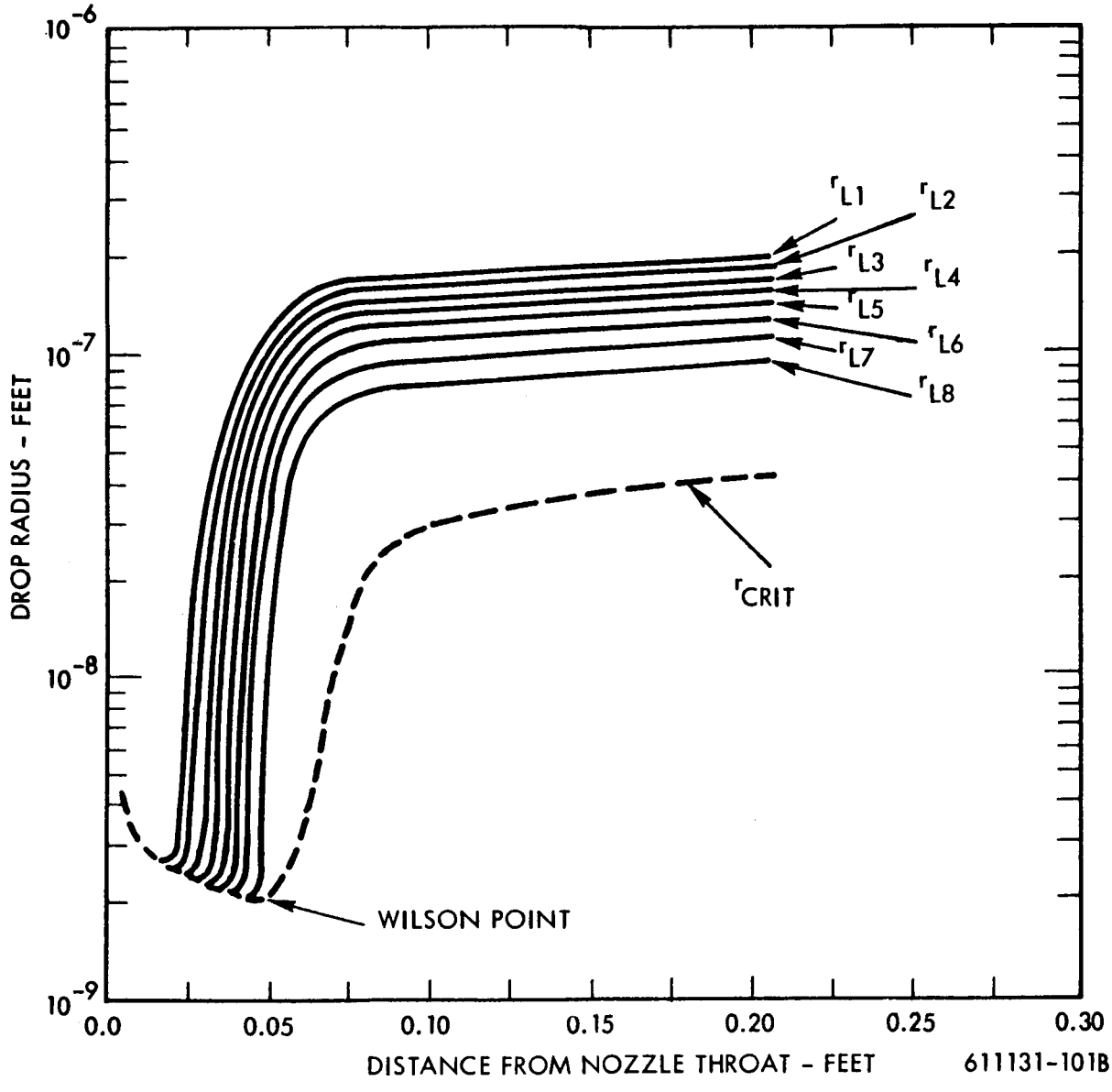

Figure B-8. Droplet Growth in Divergent Portion of Nozzle

TABLE B-4

Comparison of Condensation-Performance Program

Results with Equilibrium Expansion at Mean Diameter for the Yankee Turbine

	Condensation-Performance Program Polytropic Efficiency $\eta_p = 1.0$				Steam Division Program Equilibrium Moisture			
	Pressure (psia)	Axial Velocity (fps)	Temperature (^{o}F)	Moisture	Pressure (psia)	Axial Velocity (fps)	Temperature (^{o}F)	Moisture
Inlet	57.5	119.7	269		59.2		292	0.010
Stator No. 1	50.7	165.8	247		51.9	165	283	0.017
Rotor No. 1	44.4	183.3	258	0.0165	45.3	180	274.9	0.0240
Stator No. 2	39.0	196.1	264	0.0303	39.7	192	267	0.0310
Rotor No. 2	34.3	199.8	257	0.0374	34.9	198	259	0.0380
Stator No. 3	30.6	192	250.5	0.0438	30.5	196	251.3	0.0440
Rotor No. 3	27.0	195	243	0.04997	26.5	202	243.2	0.0500

of drops formed per pound of mixture was 3.19×10^{14}. All droplets formed by the homogeneous nucleation are within a small size range by the time the third stage is reached. As the flow proceeds through the turbine, the spread between maximum and minimum sized droplets decreases. This is explained by noting that they all have approximately the same lifetime and that smaller droplets tend to grow slightly faster than larger ones.

Calculations based on equilibrium moisture were carried out for the remaining six stages in the turbine. These mean droplet sizes are presented in table B-5.

In addition to the adiabatic frictionless case, ($\eta_p = 1$), calculations were carried out for the first stage with an assumed polytropic efficiency $\eta_p = 0.85$. This resulted in a slight delay of the Wilson point and a reduction of the expansion rate at which the Wilson point occurred. The distribution among the relative sizes was very much like that for the case $\eta_p = 1.0$, and likewise the size range is expected to be quite small. The total number of droplets generated was 1.98×10^{14} droplets per pound. The mean droplet sizes based on equilibrium moisture are also given in table B-4 for the case $\eta_p = 0.85$. The latter polytropic efficiency was applied to the actual turbine.

Condensation Results for Potassium Turbine

The same set of equations and computer program used to describe the steam condensation was also used to predict condensation in the potassium turbine. In the present analysis, as well as those of Glassman[10] and Hill[11], it was assumed that condensation of liquid metal vapors is determined by the same mechanisms as water vapor. One important influence which is believed to affect the nucleation process and the location of the Wilson point is the association of liquid metal vapors. Frisch and Willis[15] neglect the thermodynamic influence of association and theoretically predict increased nucleation rates. Katz, Saltsburg, and Reiss[16] predict a decrease in nucleation rate by including the thermodynamic effect. Their modified theory would delay the Wilson point relative to the present analysis.

The inlet potassium vapor was also assumed to be supersaturated with 1 percent equivalent moisture.* The results of the condensation performance program are compared with the

*An alternate and a more conventional assumption would be to assume the vapor to be 'dry and saturated' at the inlet. We vacillate between these two assumptions.

TABLE B-5

Mean Droplet Diameter Based on Equilibrium Moisture and Number of Drops Obtained from Condensation Performance Program for Yankee Turbine

	$\eta_p = 1.0$	$\eta_p = 0.85$
	Mean Diameter (Microns)	Mean Diameter (Microns
1st Stator	--	--
1st Rotor	--	--
2nd Stator	--	--
2nd Rotor	0.470	0.568
3rd Stator	0.495	0.595
3rd Rotor	0.520	0.620
4th Stator	0.540	0.648
4th Rotor	0.560	0.670
5th Stator	0.580	0.695
5th Rotor	0.600	0.720
6th Stator	0.620	0.738
6th Rotor	0.635	0.757
7th Stator	0.650	0.785
7th Rotor	0.670	0.806
8th Stator	0.695	0.834
8th Rotor	0.710	0.853
9th Stator	0.730	0.877
9th Rotor	0.755	0.908

TABLE B-6

Comparison of Condensation and
Equilibrium Performance Calculations for Potassium Turbine

	Condensation Performance Program				Equilibrium Calculations			
	Static Pressure (lb/in^2)	Axial Velocity (ft/sec)	Static Temperature (°R)	Condensed Moisture Fraction (lb/lb)	Static Pressure (lb/in^2)	Axial Velocity (ft/sec)	Temperature (°R)	Condensed Moisture Fraction (lb/lb)
Inlet	38.2	360	1966	0	38.2	--	2060	0.01
*Stator 1	31.3	296	1882	0	28.1	346	1987	0.035
*Rotor 1	26.5	372	1966	0.04	22.6	408	1940	0.048
*Stator 2	24.2	269	1954	0.047	15.9	398	1869	0.069
*Rotor 2	--	--	--	--	11.9	543	1811	0.085

*Conditions at exit of row

equilibrium calculations in table B-6. There is considerable disagreement between the two sets of calculations, which is, for the most part, due to the difference between supersaturated and equilibrium flow. Supersaturated flow has greater density than the equilibrium flow and was assumed to have a specific heat ratio of 1.6. Since the equilibrium flow has an effective specific heat ratio near 1.2,[17] there are appreciable differences in expansion characteristics.* Additional differences are due to slight disagreement in area ratios.

The condensation is predicted to occur in the first rotor passage with the Wilson point being reached at 68% of the axial distance through the rotor. The theoretical moisture was 3.72% at the Wilson point and P as 3000/sec which is a rapid expansion rate. The drop size distribution at the end of the first rotor is given in table B-7. The total number of drops per pound was 3.6×10^{15}, and the average diameter was 0.238 microns at the exit from the first rotor.

*Actual endurance testing of the G. E. Two-Stage Potassium Test Turbine was at turbine inlet temperatures of about 1940°R. In addition, fluid path measurements of temperatures and pressures are reported[3] only at inlet and exit of the turbine so that no experimental check on the interstage calculated values of table B-6 is currently available.

TABLE B-7

Moisture and Drop Size Distribution at Exit from First Stage Rotor of Potassium Turbine

Group	Number of Drops	Droplet Diameter, (Microns)	Moisture Fraction
1	7.3×10^{11}	0.384	0.00003
2	2.8×10^{12}	0.362	0.00011
3	1.3×10^{13}	0.339	0.0004
4	4.3×10^{13}	0.321	0.0012
5	1.5×10^{14}	0.295	0.0032
6	6.2×10^{14}	0.268	0.0097
7	2.8×10^{15}	0.223	0.0252

The calculations were performed for a second case with all properties and turbine dimensions as before except that surface tension was reduced by 20%. In this case, condensation occurred at about two-thirds of the way through the first stator. The Wilson point occurred at 2.5% theoretical moisture and the expansion rate was $\dot{P} = 1700/\text{sec}$. The total number of drops formed was 6.68×10^{15} per pound. Thus, a lower surface tension has the effect of shifting the Wilson point toward saturation, and also of increasing the number of drops formed. There were almost twice as many drops formed for the case of reduced surface tension even though the expansion rate was much lower. The pressure drop and axial velocity at exit from the first rotor were in better agreement with equilibrium calculations for this case since the condensation occurred in the first stator.

3.2 Vapor Boundary Layer Flow and Wakes

Boundary layer calculations were performed by a Westinghouse Steam Division computer code based on the method of Truckenbrodt[18]. The main equation used is adapted from the original Truckenbrodt equation for the case of turbulent flow along the entire length of the blade. Though it is disputable to ignore the laminar flow at the leading edge of the blade, this does not appear to have an appreciable effect on the calculation. Further, it is implied that laminar flow does not occur in the actual turbine due to the turbulence and unsteady flow at the inlet of the blade row, contrary to the situation in the turbine cascade where there is undisturbed flow to the blades[19].

Calculated values for the Yankee steam turbine are shown in table B-8 for the boundary layer thickness and form factor at the trailing edge of the eighth rotor and ninth stator blade rows at the 3/4 blade height position. The boundary layer thickness is found to be roughly 40% higher in the case of the rotor blade due in large part to the lower blade Reynolds Number (249,000 versus 610,000). Values also are shown for the Reynolds Number based on momentum thickness, the skin friction coefficient, and the shearing stress. These quantities are local blade surface values for the trailing edge position and are based on conventional turbulent boundary layer relations.

Similar calculations, performed for the second stator blade row of the two-stage potassium turbine, are tabulated in Volume II. The boundary layer thickness and vapor film Reynolds Number are less for the potassium turbine than for the steam turbine. This is primarily due to the smaller chord length of the potassium turbine blades. The shearing stress (τ) in the potassium turbine is much greater, by a factor of 10, because of the higher density in the potassium turbine compared to the back end of the steam turbine. The friction factor (C_f) of the potassium turbine is higher, and is associated with the thinner boundary layer thickness.

TABLE B-8

Calculated Boundary Layer Properties, Yankee Turbine*

		θ/ℓ	H	δ^*/ℓ	δ/ℓ	δ -in.	n	Re_θ	C_f	τ -ppsf
Eighth Rotor Blade at 3/4 Blade Height	Pressure Side	0.001180	1.41	0.001664	0.00978	0.0308	4.88	294	0.00606	0.677
where D=125.3", l=3.15" and Re_ℓ=2.49 x10^5	Suction Side	0.003831	1.55	0.005938	0.02747	0.0865	3.64	955	0.00348	0.390
	Total	0.005011	—	0.007602	0.03725	0.1173	—	—	—	—
Ninth Stator Blade at 3/4 Blade Height	Pressure Side	0.00829	1.41	0.001168	0.00686	0.0761	4.88	532	0.00504	0.392
where D=137.0", ℓ=11.1" and Re_ℓ=6.1 x 10^5	Suction Side	0.002705	1.51	0.004085	0.02013	0.2234	3.92	1740	0.00317	0.246
	Total	0.003534	—	0.005253	0.02699	0.2995	—	—	—	—

Where:

$$Re_\ell = \frac{V \rho \ell}{\mu}; \quad n = 2(H-1); \quad Re_\theta = \frac{V \rho \theta}{\mu}; \quad C_f = \frac{\tau}{1/2\, \rho\, V^2} = 2 \times 0.123 \times 10^{-0.678H} \times Re_\theta^{-0.268}$$

θ, δ^*, and δ are the momentum thickness, displacement thickness, and full (actual) thickness of the boundary layer at the trailing edge of the blade.

* All values are point values for the blade surface trailing edge position, e.g., C_f is the local skin friction coefficient at the trailing edge position.

Blade Wake Calculation

Downstream wakes are calculated from the boundary layer properties at the trailing edge of blades by methods as in NACA-TN 3771[20]. By these procedures the downstream properties of turbulent, low-speed wakes are specified by theoretical and empirical relations. While the experimental data is largely for isolated airfoils, there is reasonable agreement with limited cascade data.

The momentum thickness of the wake ($\hat{\theta}$ = momentum thickness/throat opening) and direction of flow (α) with respect to downstream distance is specified by analytical expressions based on continuity, energy, and momentum expressions, incompressible flow, and boundary conditions at the trailing edge of the blade. The expressions could be programmed for the computer, but in these turbine calculations, values of $\hat{\theta}$ and α were extrapolated from curves in NACA TN 3771. This approximation is justified by the small increase in $\hat{\theta}$ and α with downstream distance (roughly 2% and 0.2 degree).

While the incompressible flow assumption made in carrying out the calculations was not investigated, it is improbable that it has an important effect in well ordered turbines with thin boundary layers and, hence, only a small percentage increase in momentum thickness downstream of the blade is expected.

Results for the ninth stator of the Yankee steam turbine are given in figure B-9. Results for the eighth rotor and for the second stator of the two-stage potassium turbine are given in Volume II. As shown, the wake properties (H, α , δ) quickly change downstream of the trailing edge--whereby there is little change beyond 0.1 to 0.2 x/ℓ. Note also that while the wake thickness (δ) continues to increase beyond 0.1 to 0.2 x/ℓ, the velocity within the wake (V(y)) is nearly the same as that of the free stream since:

$$V(y) = V(x) \left(\frac{y}{\delta} \right)^{\frac{1}{n}} \text{ where } n >> 1. = \frac{2}{H-1.} \quad *$$

Thus, the downstream flow is roughly axisymmetric from about 20% of the chord length distance downstream of the blade by this model of the process. Because of the relative size of the two turbines, the thickness of the wake from the steam turbine blades is an order of magnitude greater than from the potassium turbine blades.

---

*See figure B-9

x/ℓ	H	$\hat{\theta}$	α	θ-in. $\frac{\hat{\theta}\ell \sin\alpha}{\sigma}$	n $\frac{2}{H-1}$	δ-in. $\frac{\theta(1+n)(2+n)}{n}$	V(x) fps	V(y) fps
Pressure side								
0 (t.e.)	1.41	0.00369	25.3	0.009196	4.88	0.0763	955	
0.05	1.202	0.00372	25.2	0.00927	9.90	0.1212	948	
0.1	1.15	0.00372	25.2	0.00927	13.35	0.153	935	
0.2	1.107	0.00372	25.2	0.00927	18.70	0.202	935	
0.358 (Rotor Inlet)	1.08	0.00372	25.2	0.00927	25.0	0.260	935	$V(y) = V(x)(y/\delta)^{1/n}$
Suction side								
0 (t.e.)	1.51	0.01206	25.3	0.03003	3.92	0.223	995	
0.5	1.24	0.01222	25.1	0.0304	8.34	0.352	948	
0.1	1.177	0.01222	25.1	0.0304	11.30	0.440	935	
0.2	1.127	0.01222	25.1	0.0304	15.80	0.575	935	
0.358 (Rotor Inlet)	1.095	0.01222	25.1	0.0304	21.10	0.735	935	

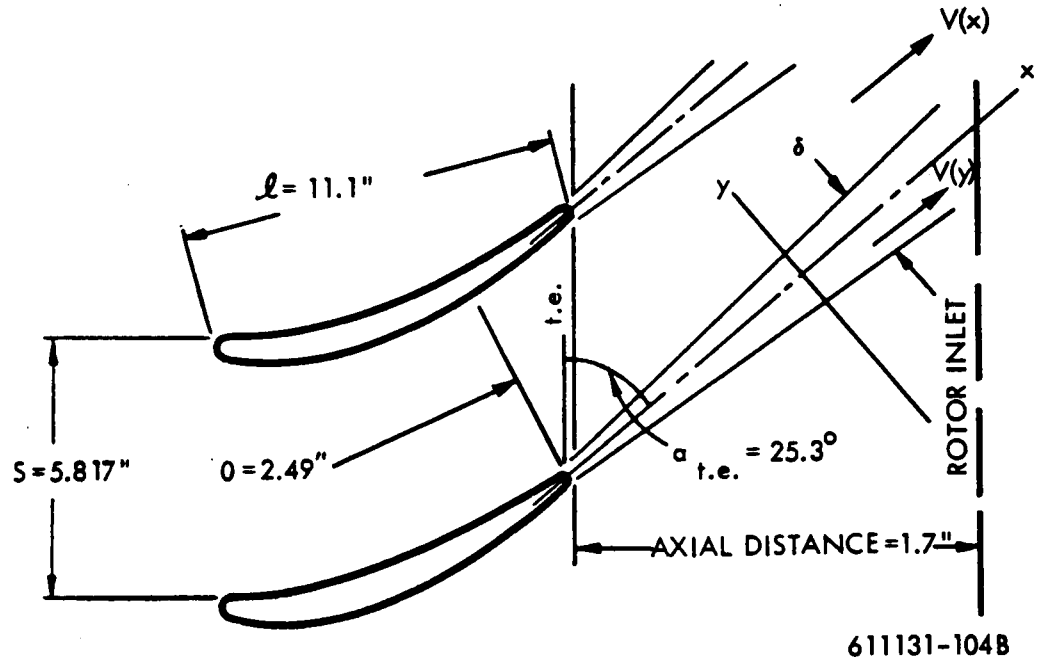

Figure B-9. Results of Blade Wake Calculation for Ninth Stator Blade at 3/4 Height Position, Yankee Turbine

Possibly, the greatest weakness in this calculation is in regarding the wake as a viscous process associated with the trailing edge boundary layer. Generally, this is only correct for near zero trailing edge thickness as in the Lieblein report.[20] In actual turbines, the wake from the trailing edge of the blade is, generally speaking, like the separated vortex flow downstream of a circular cylinder. Investigations by Heskestad[21], as well as current Westinghouse tests, show that the downstream wake depends to a large extent on the detailed geometry of the trailing edge. Strong vortex streets are associated with thick, cylindrical trailing edge shapes. Information such as that given in figure B-9 may be plotted in the form shown in figure B-10. This particular plot is for a zero trailing edge thickness as this is the analytical model available. The chief use of information of this kind in the overall model of erosion is to estimate the amount of atomization and acceleration of the liquid collected on a stator in the interval (both time and distance) between the stator and rotor. To compensate for the finite trailing edge thicknesses of actual apparatus in making these aforementioned calculations, the wake was treated mathematically as a dead space 4.8 trailing edge thicknesses in length joined to a zero trailing edge thickness wake at a discontinuity. The discontinuity is represented by the vertical line in figure B-10. A justification of this procedure is that trajectory calculations agree favorably with the scant experimental information available.[25] (See Vol. II, Section D.)

3.3 Deposition of Moisture on the Surface of Blades

The deposition of moisture is considered from the standpoint of: (1) the deposition on the inlet edge (nose) of the blades and (2) the deposition on the concave face of the blades. The mechanism of deposition of moisture on blade surfaces is considered to be that of inertial impaction based on the macroscopic application of the laws of motion. In this we have followed Gyarmathy. While deposition by diffusion of particles (Brownian motion and/or eddy diffusion) is recognized as a possible factor, inertial impaction is felt to warrant first consideration. Even between inertial impaction calculations (Gyarmathy[1] and Brun et al[22]) there is substantial difference in numerical values.

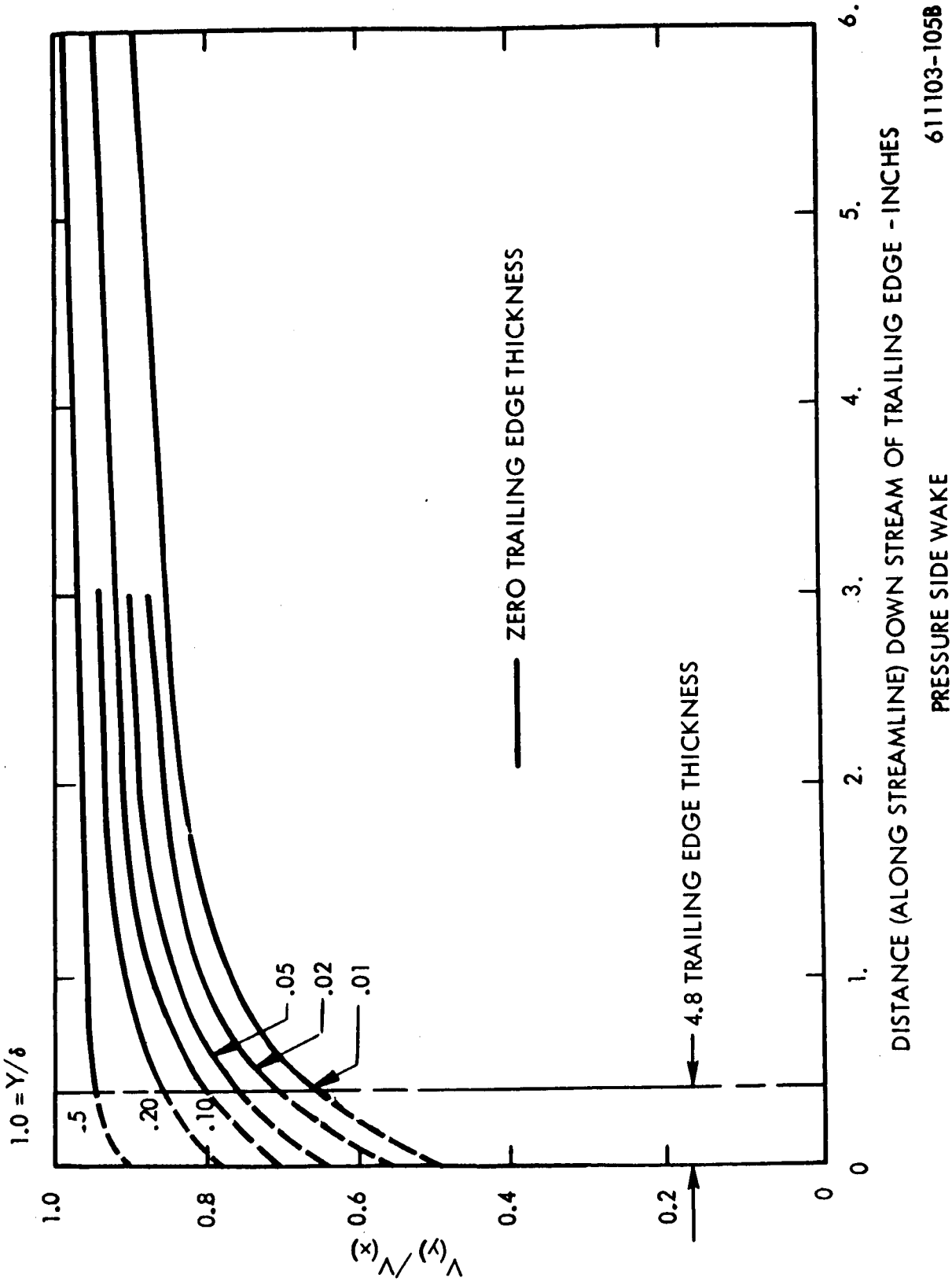

Figure B-10. Wake Pressure Side Velocities, Ninth Yankee Stator

Deposition on the Inlet Edge of the Blades

The analysis considers the nose of the blade as a circular cylinder. Thus, the impingement of moisture particles is specified by the path of the particles when acted upon by the potential flow about a circular cylinder. The path and impingement of particles with respect to circular cylinders, based on two-dimensional trajectory calculations and suitable drag coefficients, are specified by a number of reports. NACA report 1215[22] was used.

As the flow about the miniature moisture drops is often in the slip flow regime, it is necessary to correct the NACA data for the reduction in drag due to slip flow. Correction was made by multiplying the report value of the inertia parameter by the ratio ($C_{D,\ slip\ flow}/C_{D,\ continuum}$) where C_D is the conventional drag coefficient for continuum flow. This correction is specified by an empirical expression in terms of Knudsen number.[23]

By these data, the collection efficiency was calculated for the nose of the ninth stator blade row, 3/4 blade height position, Yankee steam turbine, and is shown in figure B-11. For comparison, the efficiency is also shown by Gyarmathy's data. These data give a higher collection efficiency throughout the range of moisture drop size. This difference cannot be explained by the fact that the NACA data account for the increase in Stokes' law drag with Reynolds Number since, in this instance, the fluid properties are nearly coincident with the NACA curve for zero Reynolds Number (φ = 0.). Possibly, the difference could be explained by differences in the trajectory calculation, but this calculation is not qualified in Gyarmathy's report.

By the NACA curve, drops less than 0.3μ radius do not collect on the nose of the blade, but, by Gyarmathy's curve, the collection efficiency is roughly 15% for 0.4μ estimated drop radius.

The portion of drops collected on the inlet edge is shown in figure B-12. The portion with respect to the total number of drops depends on the collection efficiency and the size of the blade inlet edge. By the NACA curve, drops less than 0.3μ radius are not collected, but, by Gyarmathy's curve, 0.5% of the drops are collected on the nose of the blade for 0.3 μ radius.

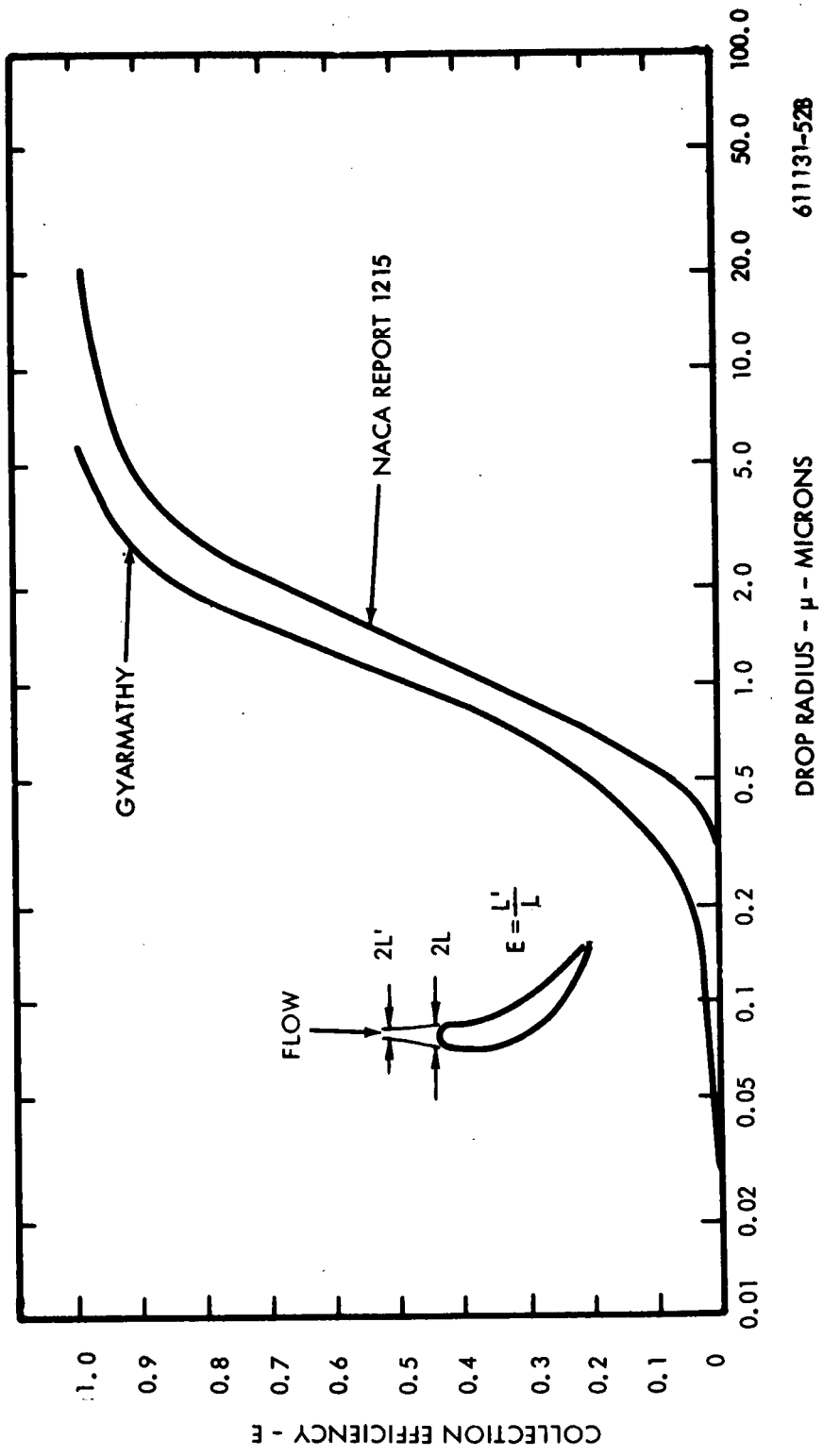

Figure B-11. Collection Efficiency, Ninth Stage Stator Nose Yankee Turbine

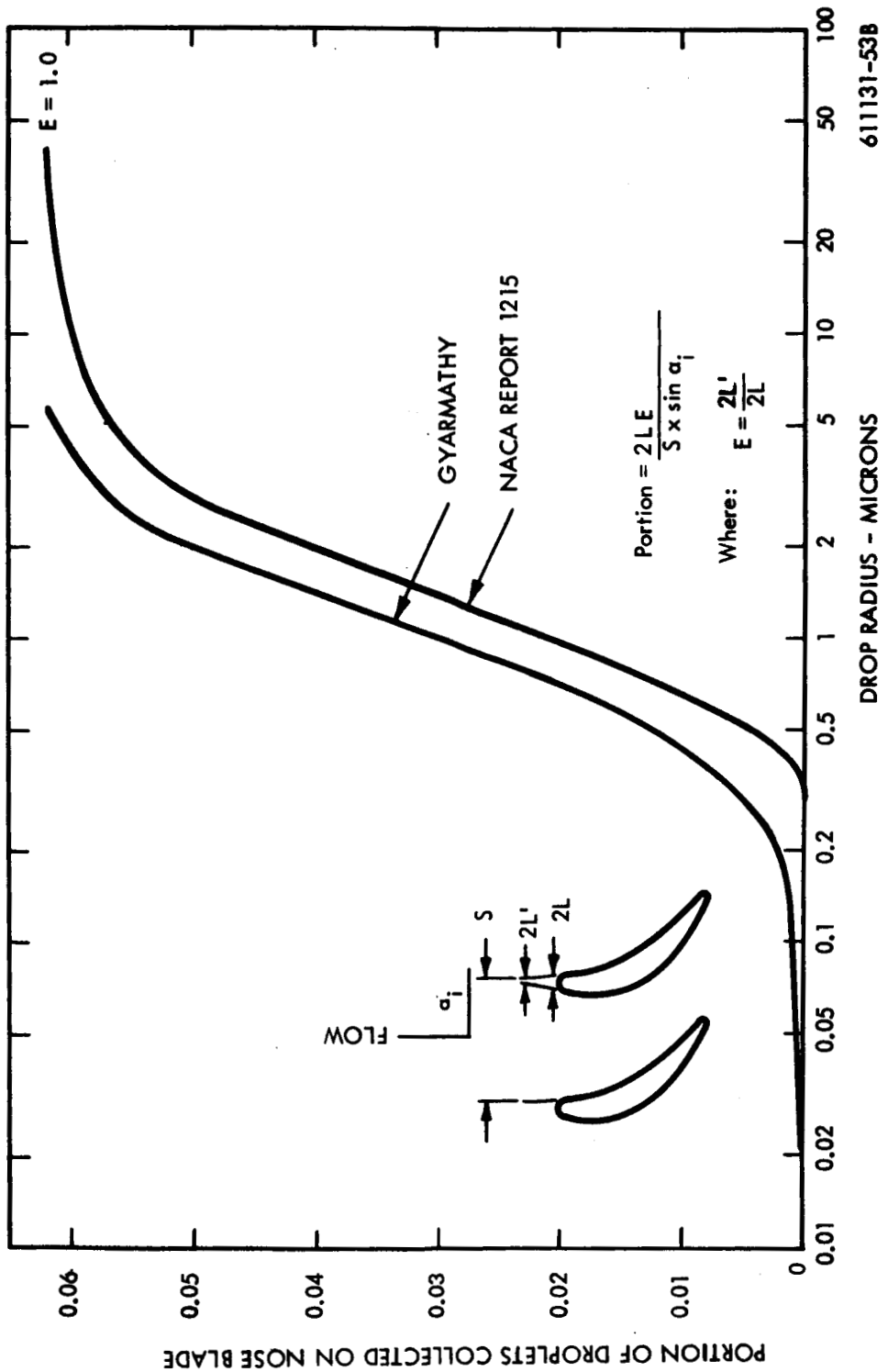

Figure B-12. Portion Collected, Ninth Stage Stator Nose Yankee Turbine

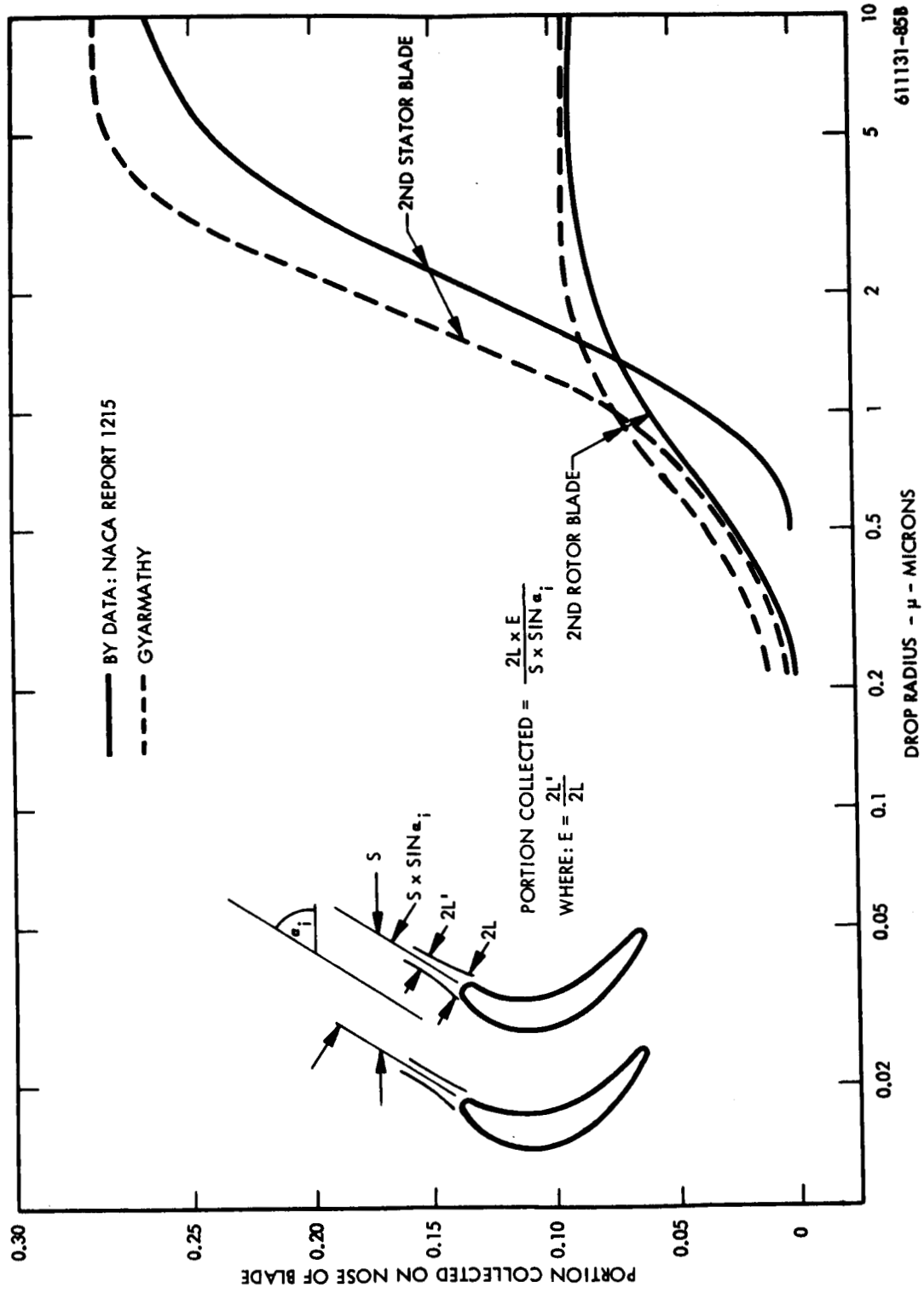

Figure B-13. Two-Stage Potassium Turbine Portion Collected 2nd Stator Nose

A similar situation exists with respect to the collection calculations on the blade noses of the two-stage potassium turbine. Figure B-13 gives the portion collected on the second state stator and rotor. For a 0.25μ drop size, about 0.2% of the drops are collected on the nose of the rotor blade. Drops < 0.5μ are not collected on the nose of the stator blade. A larger collection is shown by the Gyarmathy data due to the higher collection efficiency. While the density of liquid potassium, which is about 2/3 that of water, tends to reduce the collection on the inlet edge, the greater part of the difference in the steam and potassium turbine is accounted for by the size of the inlet edge relative to the total passage size.

Deposition of Moisture on the Concave Face of the Blade

The analytical approach was similar to that of Gyarmathy. The contour of the blade surface was approximated by a polynomial expression. The path of the vapor was assumed to correspond to the blade contour. The path of moisture particles acted upon by the drag of the vapor was calculated by the trajectory equations. The drag on the particles is by Stokes' law with correction for slip flow. By simplifying assumptions of constant vapor velocity with respect to the space between blades and equal and constant moisture-particle axial velocity, the particle acceleration was described by a linear differential equation. By further assumptions as to boundary conditions, the integrated equation gives the width of the band, at blade inlet, within which all moisture particles impinge on the blade surface. Finally, the ratio of band width to the space between blades gives the amount collected with respect to the total moisture approaching the blades.

Thus, from the above assumptions, the collection of moisture is specified by closed form calculation. Since this treatment of the process is not covered in the literature, a detailed account of the equations is given in an Appendix to Volume II.

Calculation results for the Yankee steam turbine are shown in figure B-14. This figure shows the portion of moisture collected as a function of drop size. The portion collected is specified by the inlet width of the band (ξ), within which all particles impinge on the blade with respect to the blade pitch. The band width cannot exceed

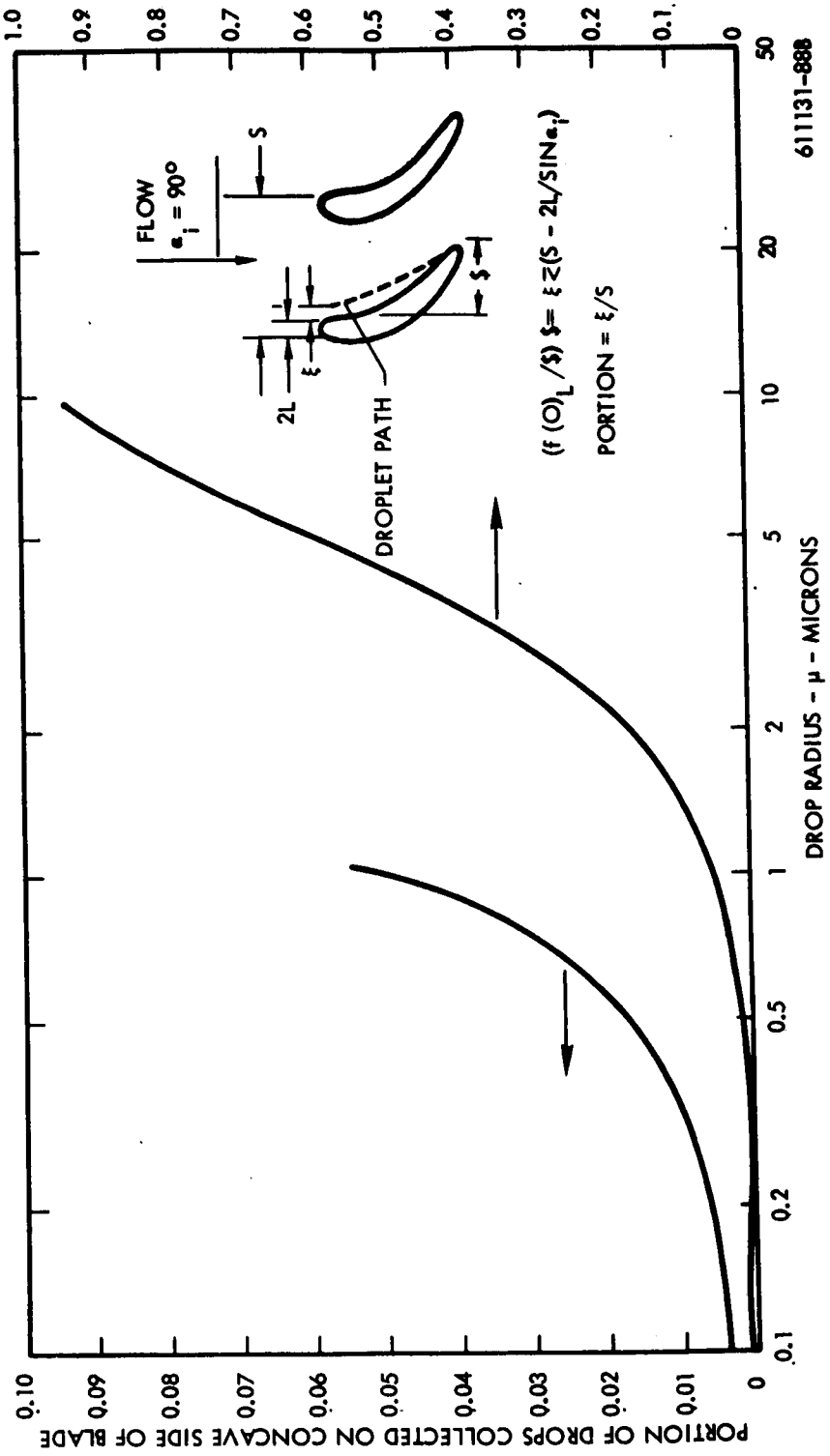

Figure B-14. Portion of Drops Collected Concave Side Ninth Stator
Yankee Turbine

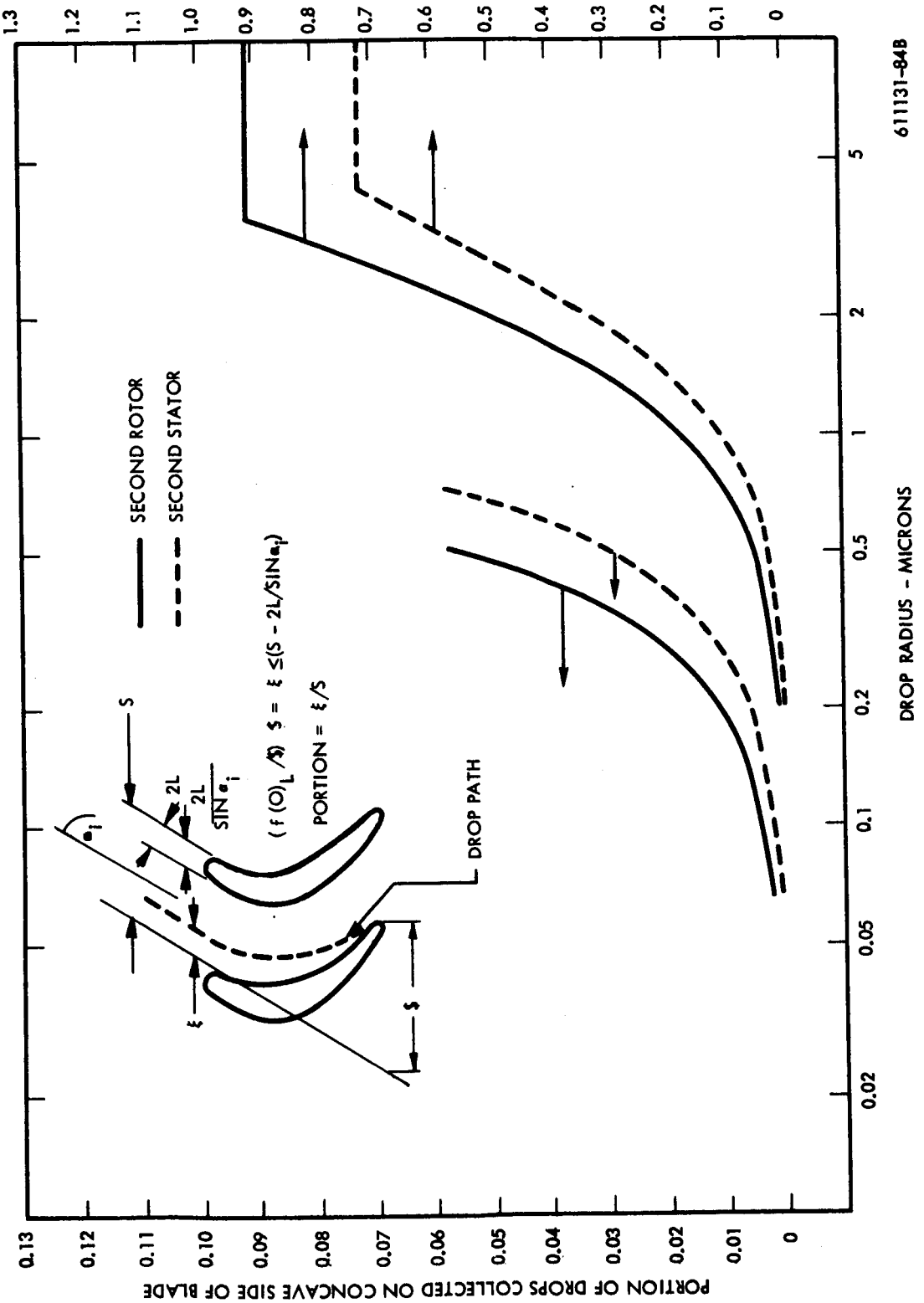

Figure B-15. Portion of Drops Collected Concave Side Two-Stage Potassium Turbine

the space between blades (pitch minus inlet edge blockage) which accounts for the break in the curve at 93-1/2%. Collection by Gyarmathy's data is 20% less in the range <0.4μ drop size. The difference is due to the fact that Gyarmathy specifies the blade shape by a quadratic expression compared to a higher order curve fit in the present analysis. This more closely matches the shape of the ninth stator blade.

For 0.4μ estimated drop radius, 1.3% of the drops are collected on the concave side of the blade by Gyarmathy's data the portion collected is 1.04%. Similar calculations were carried out for the two-stage potassium turbine. Figure B-15 gives the portion of moisture collected on the concave side of the second stage rotor blade. The calculation assumes a blade surface shape as by the average between a second and third degree polynomial and drag on the drops as by Stokes' law with correction for slip flow. As shown in the curve, the portion collected is specified by the width of the band (ξ), within which all particles impinge on the blade with respect to the blade pitch(s). The band width cannot exceed the space between blades (pitch minus inlet edge blockage) which accounts for the break in the stator and rotor curve at 72 and 91%. Collection by Gyarmathy's data is nearly the same and is not shown.

For 0.12μ radius drops, 0.3% of the drops are collected on the stator blade surface and 0.6% on the rotor blade surface. The larger collection on the rotor surface is primarily due to the passage shape (higher value of $/s). This compares to approximately 0.4% collection in the Yankee steam turbine at the same drop radius. Here, the difference is due primarily to the passage shape rather than fluid properties. (The inertia parameter is inversely proportional to the blade width, and hence, is much greater in the potassium turbine.)

3.4 Movement of Moisture on Blade Surfaces

The movement of collected moisture over the blade surfaces is not a critical part of the overall erosion model with respect to numerical precision. The analysis shows the relative importance of certain variables and provides a qualitative understanding of one of the sequence of events leading to turbine blade erosion.

It is assumed that the collected moisture forms a continuous liquid film controlled by the laws of viscous flow. The thickness and velocity of the moisture film is based on the force balance between viscous shear in the film, vapor stream friction, centrifugal force, and momentum imparted by fog drop impact. The force on such a film from the radial pressure gradient in the turbines examined is small compared to the other forces. It is also assumed that the moisture collects only on the concave side of the blades (for the purpose of numerical calculation). Collection on the convex sides through the action of secondary flows is neglected.

Calculations on the eighth rotor blade of the Yankee turbine were performed assuming 2% (of the fog present) moisture collection. The axial component of velocity was 0.88 ft/sec and the radial component, 6.5 ft/sec. This corresponds to a 7.8 degree angle of flow with respect to the radial direction. From this it is concluded that almost all the moisture collected on rotor blades will be flung from the tips to impact the turbine casing. If adequate moisture removal slots are provided there should be little carryover of collected moisture from a rotor row to the following stator row.

Similar calculations were made for the ninth stator of the Yankee turbine. The results are presented in parametric form in table B-9. The Reynolds Number is calculated using conditions at the trailing edge of the blade also. From limited data, it appears that there are ripples on the surface of the film when the film Reynolds Number is greater than 4, corresponding to ϵ greater than 1%. The presence of such ripples is a necessary, but insufficient condition to allow use of the sheet atomization model of primary atomization developed in section 3.5.

Similar calculations were carried out for the two stage potassium turbine. Results may be found in Volume II.

TABLE B-9

Yankee Steam Turbine, Ninth Stator Liquid Flow

Percent of Available Moisture Collected (ϵ)	Liquid Film Velocity ($\bar{u}$) (f/s)	Liquid Film Reynolds No. (Re_L)
0.005	0.404	1.55
0.010	0.585	3.1
0.020	0.869	6.23
0.050	1.54	15.5
0.100	2.54	31

* Velocity is the mass average value at the trailing edge of the blade.

3.5 Atomization and Trajectories of Damaging Liquid

As discussed in the preceding sections, a small percentage of the condensate drops passing through a turbine collect on the stator vanes. The collected moisture is carried to the rear of the stator vanes by the drag forces of the main stream. At and near the trailing edge of the stators the liquid is detached from the surface and ultimately forms a spray of relatively large drops. This detachment process from the stators is designated "primary atomization" in conformity to the usual terminology for gas-atomized sprays.

The drops from the primary atomization process are caught up in the decaying wake of the stator or into the bulk stream. In either case, most of the primary drops are subjected to air forces which are sufficient to disrupt them further. This additional fracturing of the collected liquid is termed "secondary atomization", also in conformity with gas-atomization terminology. In previous studies of the overall erosion process by Gardner[2] and Gyarmathy[1], the simplifying assumption is made that all the drops formed by the primary atomization processes undergo secondary breakup before impacting the turbine rotor. This study differs from these previous studies in that an attempt is made to trace the history of the relatively small percentage (about 10%-20%) of the primary drops which do not undergo secondary breakup. Unfortunately, from the point of view of model simplification, these large unbroken primary drops cause damage disproportionate to the percentage of damaging liquid involved.

Before, during and subsequent to the secondary atomization process, if time is available, the drops are accelerated along the vector of the vapor stream*. The drops arrive at the inlet of the following turbine rotor in a variety of sizes and with a dispersion of velocities relative to the nose and leading edge of the blades. It is, of course, the impacting of these drops on the rotor blades which causes the erosion damage of concern in this analytical model.

To calculate the erosion caused by this liquid, it is necessary to know the size, relative velocity and number and location of impacts on the rotor blades as a function of time. At least four different mechanisms of primary atomization, and two of secondary atomization have been observed experimentally under conditions related to those in turbine stators. There are, as well, a variety of accelerational paths provided by the velocity profiles in the stators' trailing edge wakes. To trace all possible paths and processes would be a formidable task. Therefore, a simplified approach was taken to estimate distribution of drop sizes and drop velocities of impact. This involves substantial simplification by means of the gross description of droplet classes based in part on empirical correlations from gas-atomization studies. In this investigation emphasis was placed on the processes as they might apply in the Yankee Atomic Plant low-pressure steam turbine and in particular to the last stage of that turbine. Nonetheless, it is felt that the observations in the steam turbine are applicable to a broader spectrum of turbine working fluids (such as the liquid metals) of low liquid viscosity and substantial surface tension.**

---

* Calculated time to complete secondary breakup in the Yankee turbine (ninth stator exit) using Gardner's equation is ≈ 0.5 millisecond. A representative time of flight between stator and rotor is 4 milliseconds.

** Wetability of the liquid with respect to surfaces does not seem to be an important factor. Experiments reported in Reference 24 indicate that under the impress of aerodynamic forces (even where good wetting would occur in the absence of such forces) liquids tend to become non-wetting. This is reasonable since the ground state of a liquid mass in the absence of external forces such as gravity is a sphere and perturbations from aerodynamic sources would tend to allow films and rivelets to "ball up."

The calculational procedure used to estimate the drop sizes approaching the turbine rotor inlet involved six steps. The first step was to estimate an average primary drop size. The model chosen for this purpose was the classical sheet of liquid ruffled under the impress of aerodynamic forces, the ripples developing into ligaments, and the ligaments in turn collapsing into drops. Results of calculations for the ninth stator of the steam turbine are given in figure B-16. The derivation of the numerical expressions used is given in Volume II.

Observations in an actual turbine are reported in Reference 25 and in turbine-like stationary cascades in References 25 and 24. Mechanisms of primary atomization reported are: (1) stripping of masses of liquid or sheets from liquid puddles, (2) stripping or tip bursting of oscillating pendant drops attached to the stator trailing edge, (3) eye-dropper-like tearing of individual drops from the stator trailing edge and (4) direct formation of individual drops on the convex surface of stator by some mechanism giving results similar to a drop of water on a hot stove.

In none of these references is there quantitative information on the relative volumes of liquid involved in the observed processes. It seems reasonable that the tearing of masses or sheets of liquid from the stators involves a more important part of the total liquid available than the other observed mechanisms of detachment. The sheet atomization model is on this basis the logical tool for estimation of average primary drop sizes. As the information available is not conclusive, the pendant modes may be more important than assumed. A discussion of pendant atomization is given in Volume II.

An estimate of the primary drop size distribution was obtained by applying the well-known empirical drop size distribution function of Nukiyama and Tanasawa[33] to an average primary drop size. A value of 525 microns was picked for this average drop diameter. This is an arbitrary selection based on an inspection of figure B-16. It allows for a modest amount of rivulet formation, rather than a uniform distribution of liquid flow. The distribution function was applied assuming that the average drop size estimate represented the maximum rate of creation of spray volume. This latter assumption is consistent with the assumption that the sheet model is volume-wise the most important of the primary atomization processes occurring

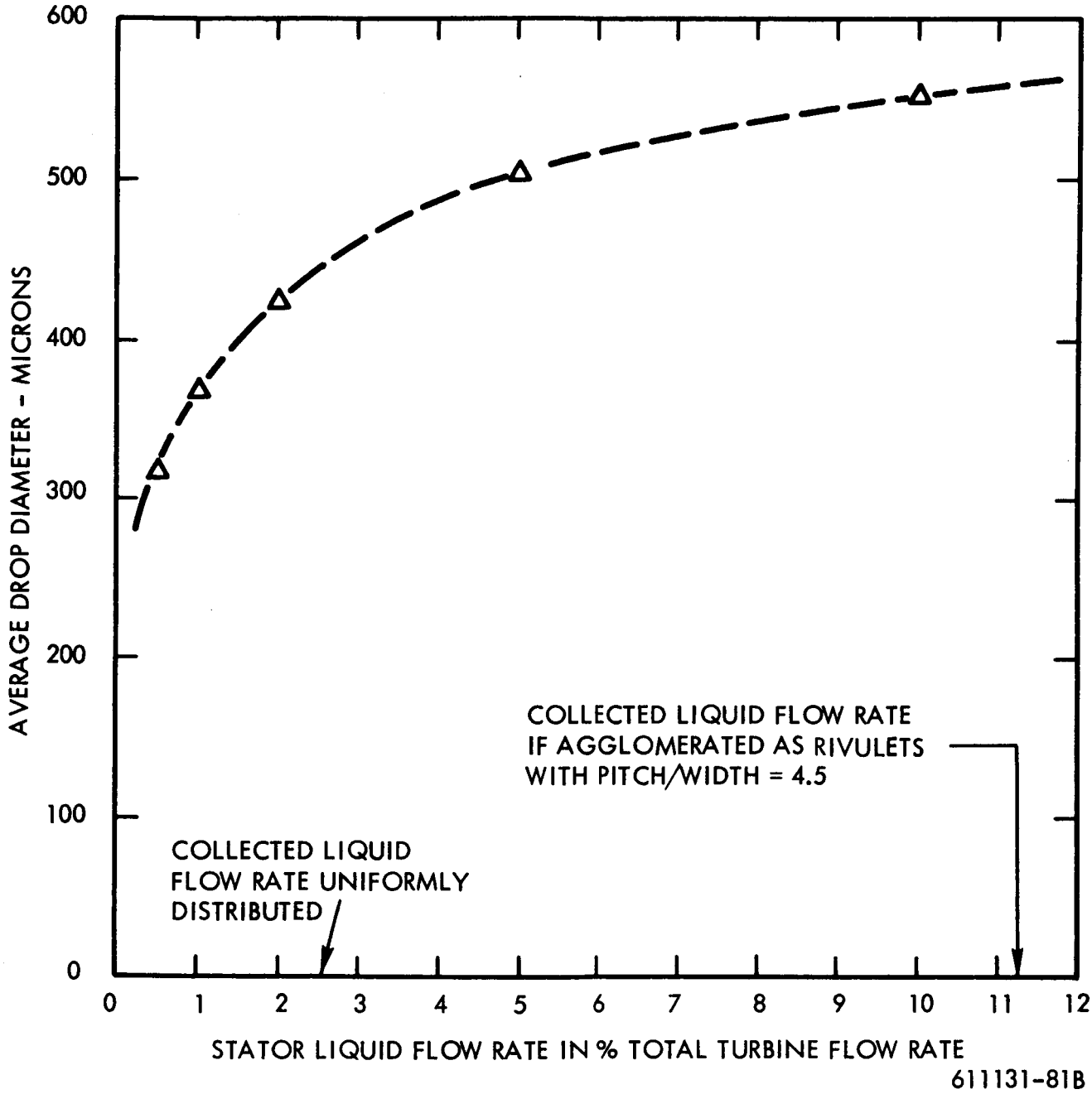

Figure B-16. Ninth Yankee Stator, Primary Atomization, Average Drop Diameter

in a turbine. Use of an empirical distribution function, to some extent, allows for the other possible processes of primary atomization, since they too will be expected to produce distribution drop sizes, and may have been present in the studies of gas atomization of liquids to which the Nukiyama-Tanasawa function has been applied as a correlating parameter. The results for the ninth stator of the steam turbine are given in figure B-17.

To distinguish between primary drops which are stable from origin to rotor impact, and primary drops which undergo secondary atomization, a two-dimensional parametric time history analysis of drops in the stator wake was performed. The parameters used were drop diameter and wake streamline path. It was assumed that the primary drops become entrained by a given wake streamline and that the liquid represented remains with that streamline until rotor impact. The criteria for disruption of a primary drop was taken as exceeding a critical drop Weber Number somewhere along the path between detachment from the stator to impact with the rotor. Because of the relatively low viscosity and density of water, it is reasonable to use a simple Weber Number criterion for maximum drop stability. However, the correct numerical value of this criterion for use in turbines has not been established. Based on the single drop experiments of others, Gardner found that it may vary from a low of about 13 (for shock conditions) to a high of 22 for a steady flow increase in velocity. As seen from the results of a particular trajectory calculation in the wake of the ninth stator Yankee turbine (figures B-18a and B-18b), the drops deep in the wake undergo conditions which resemble a steady flow increase. The conditions are assumed to be steady flow, and examination has been confined to critical Weber No. = 22. Unfortunately, calculated erosion rates are very sensitive to this parameter (Section 4).

The remainder of the collected liquid (80 to 88%) is then assumed to undergo secondary atomization to produce a mass mean drop diameter (according to the Wolfe and Andersen[26] equation) with the mass distributed among various size drops (in accordance with the Nukiyama and Tanasawa[33] distribution function). The former equation is theoretically derived and has

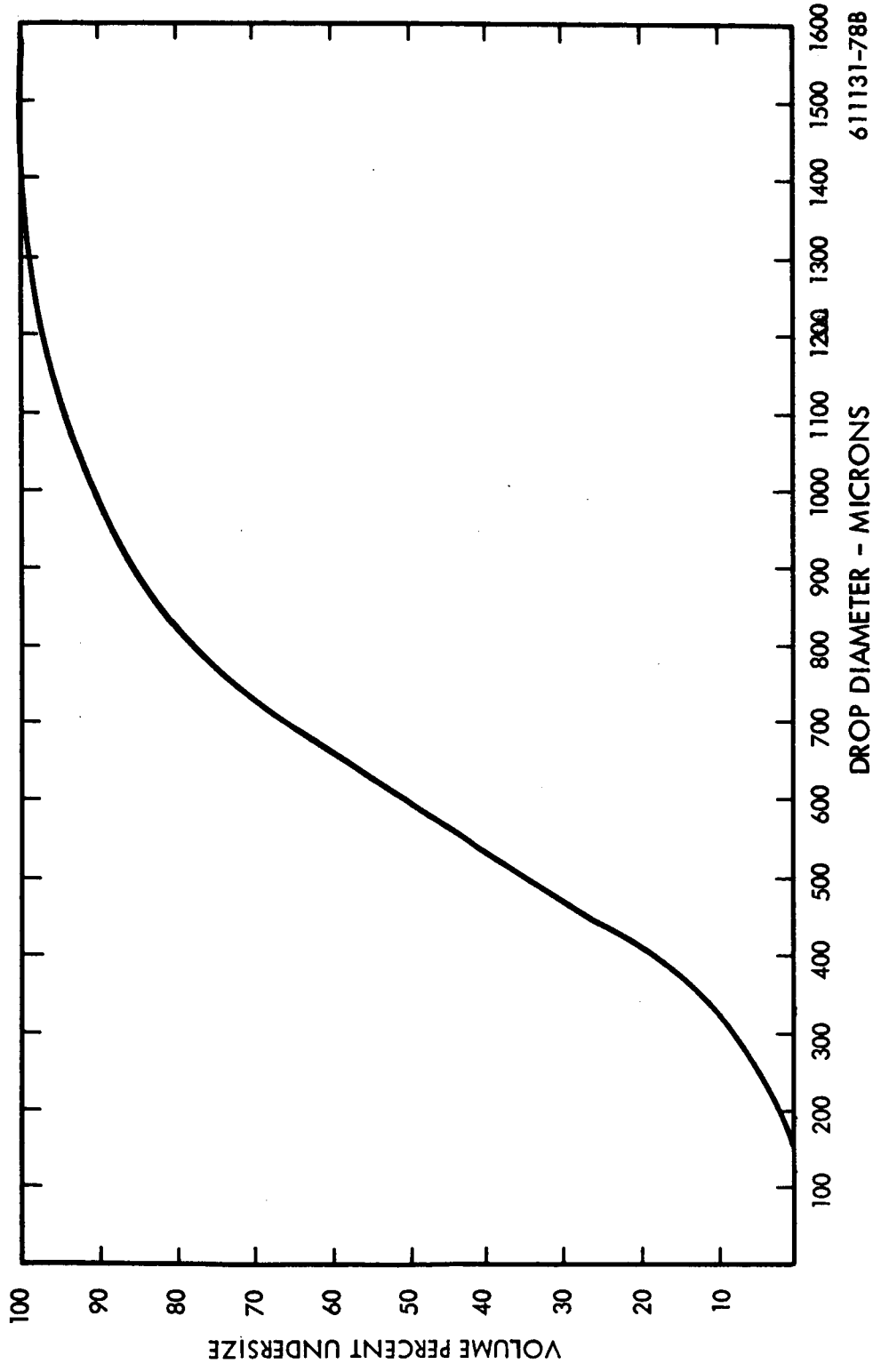

Figure B-17. Primary Atomization Distribution, Ninth Stator Yankee Turbine

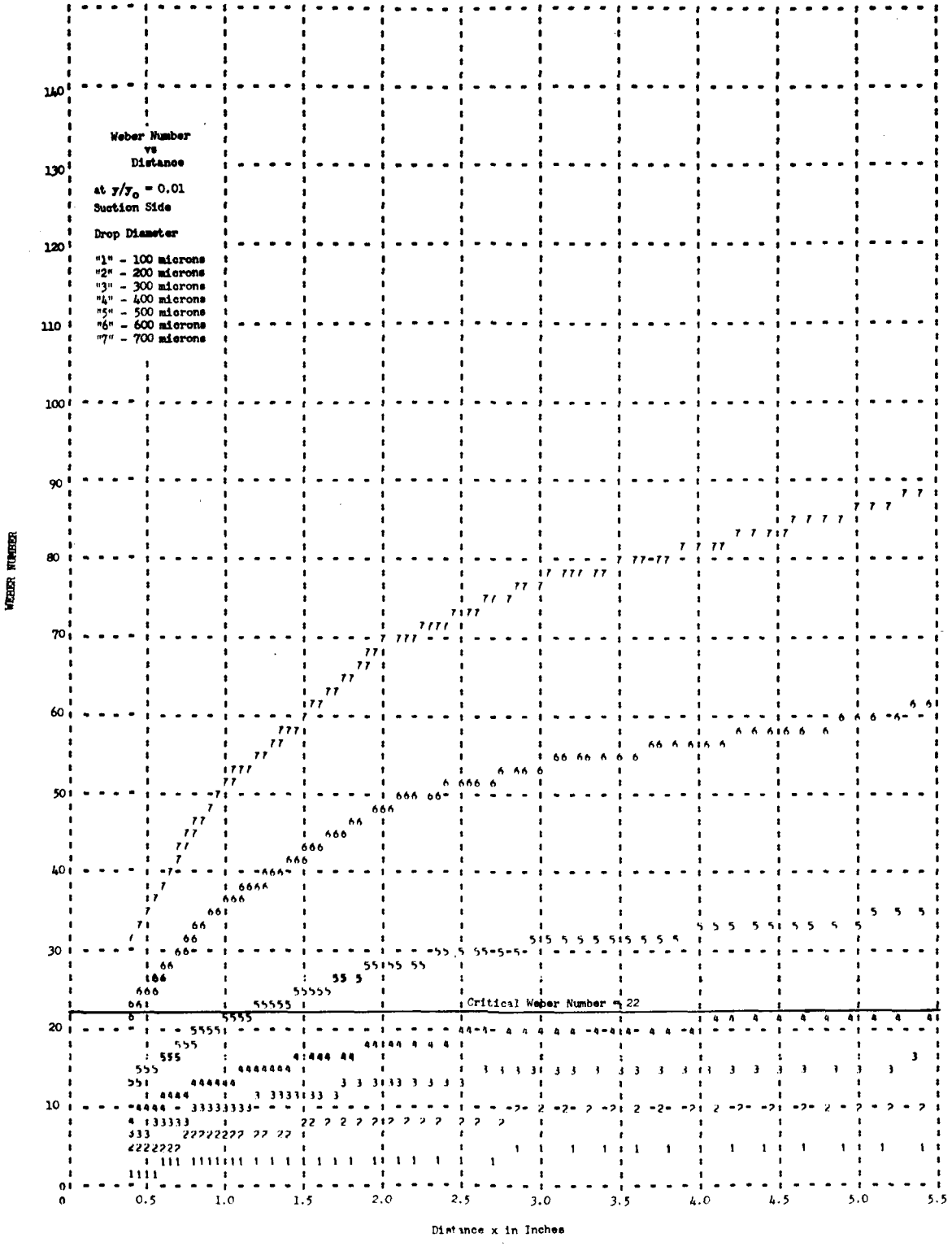

Figure B-18a. Ninth Yankee Stator Wake, Weber Number vs Distance at y/yo - 0.01 Suction Side

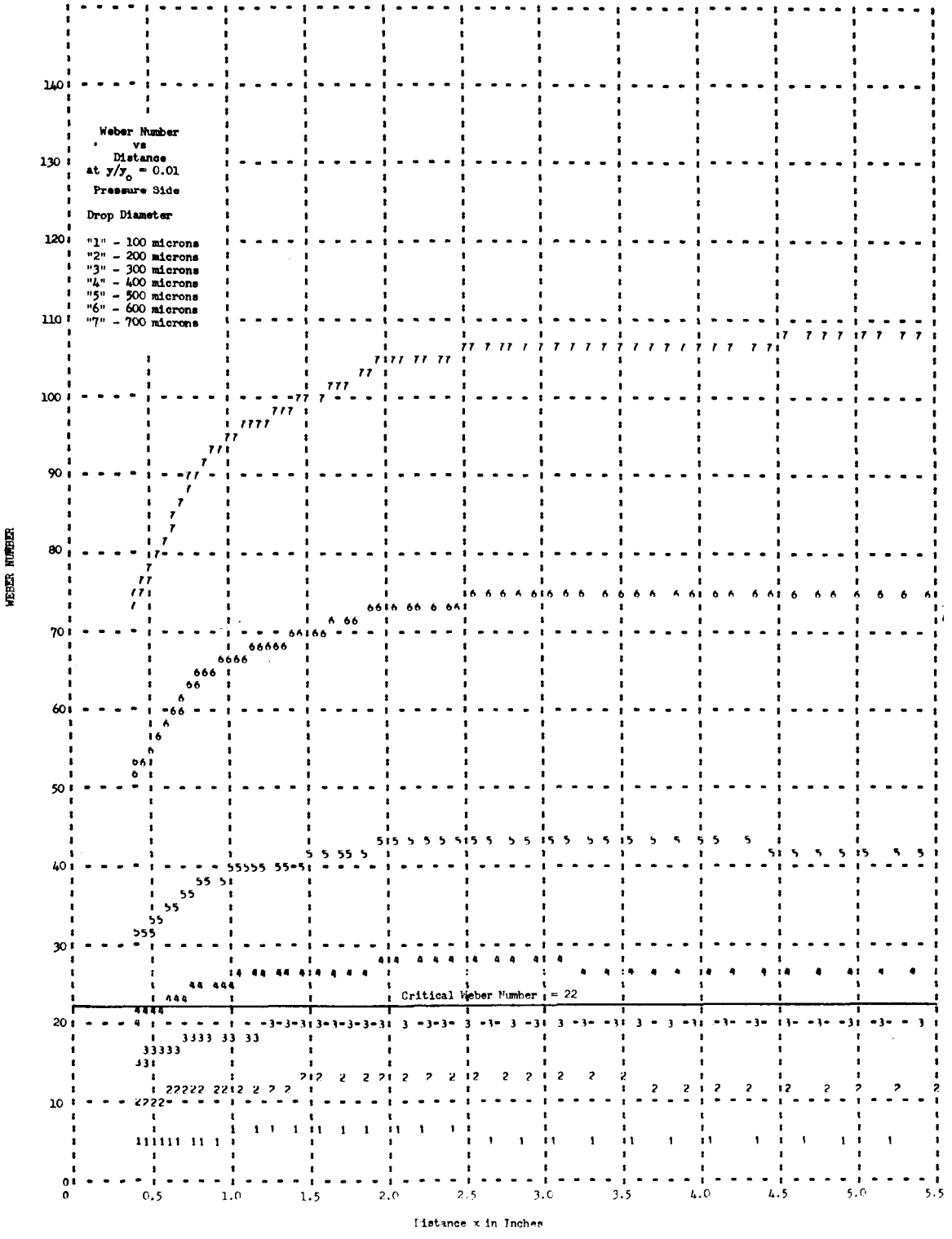

Figure B-18b. Ninth Yankee Stator Wake, Weber Number vs Distance at y/yo - 0.01 Pressure Side

limited experimental confirmation. The distribution function is an empirical one derived on the basis of the examination of a substantial number of gas atomized liquid sprays. The residual of the primary drop distribution is then added to the secondary drop distribution to give the drop size distribution arriving at the plane of the following rotor. Such a distribution for a critical Weber No. of 22 applied to the pressure side wake is given in figure B-19.

All preceding calculations were carried out across a tangential slice of the stator wake at a single radial station between hub and tip.* Since there is a substantial change in state conditions from the hub to tip of a turbine, an approximate correction to the parametric trajectory calculations was incorporated when using the information to establish the dispersion of velocities impacting the turbine rotor. It is assumed (Volume III) that the damaging component of the drop impact velocities is that normal to a blade surface. Because of radiusing of the blade nose, in the Yankee turbine, at least some drops will hit locally with a normal velocity equal to the full relative velocity between drop and rotor. To either side of this location the impacts will be oblique. Calculated values for full relative velocity impacts are given in figure B-20. Values for some of the oblique impacts are included in Volume II. Calculated lengths of the zone of drop impingement back from the leading edge of the nose and on the convex side of the Yankee ninth rotor blades are given in figure B-21. The downstream edge of this zone is set by the geometric shadowing of one blade on another as determined from the trajectory information.

The results of the trajectory and atomization calculations are in qualitative agreement with the sparse experimental information available. The erosion in the Yankee turbine is on the nose of the blade over the last two inches at the tip. There is fair quantitative agreement between the calculated drop velocities and those observed in a CERL of Great Britain stationary cascade[25] under state conditions similar to those in the Yankee turbine. In addition, there is an approximate agreement in maximum size of primary drop which can escape secondary atomization between these calculations and the reported maximum size of drops observed

* 1/2 blade height for the trajectory calculations; 3/4 blade height for primary atomization calculations.

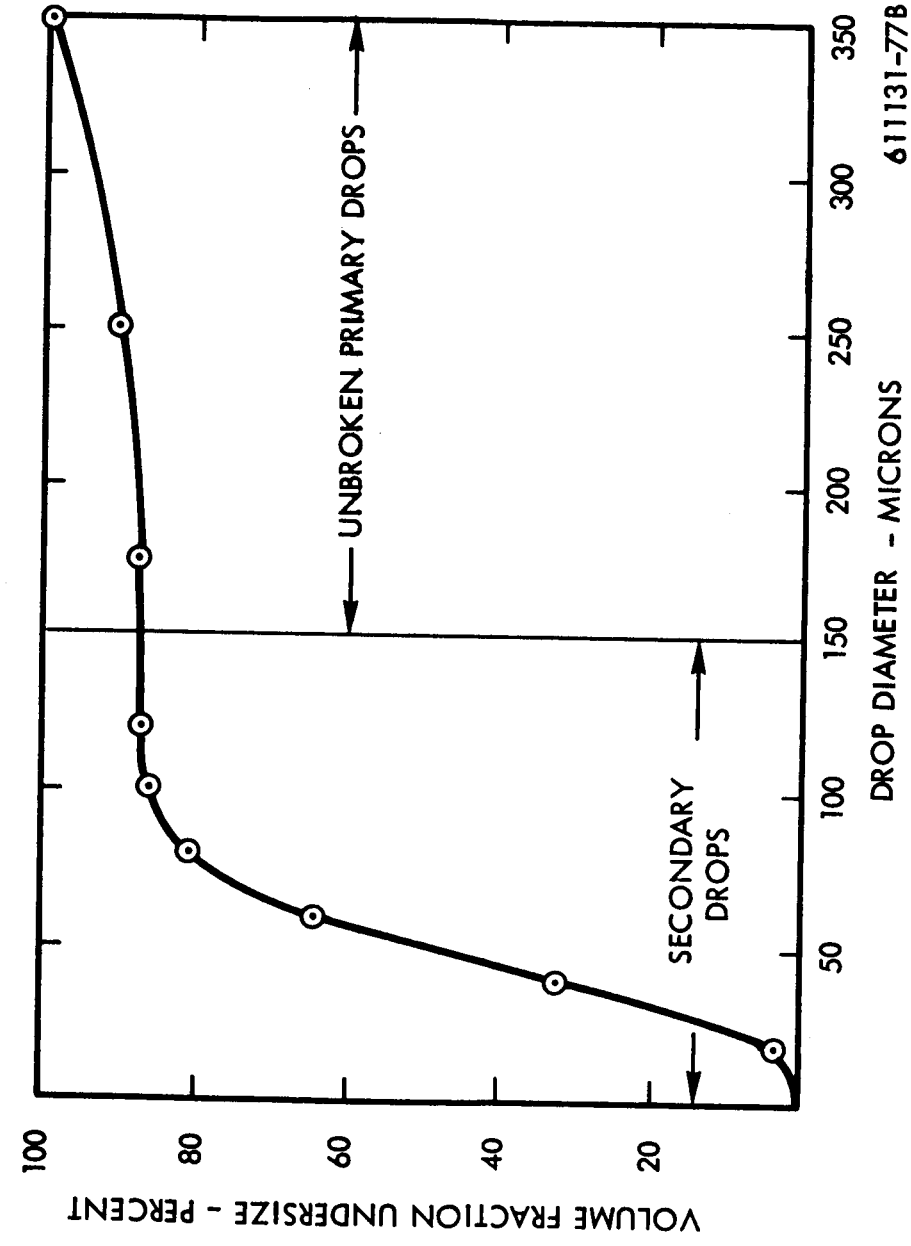

Figure B-19. Impacting Drop Size Distribution, Critical Weber No. = 22; Ninth Yankee Rotor Pressure Side Wake of Stator Calculation

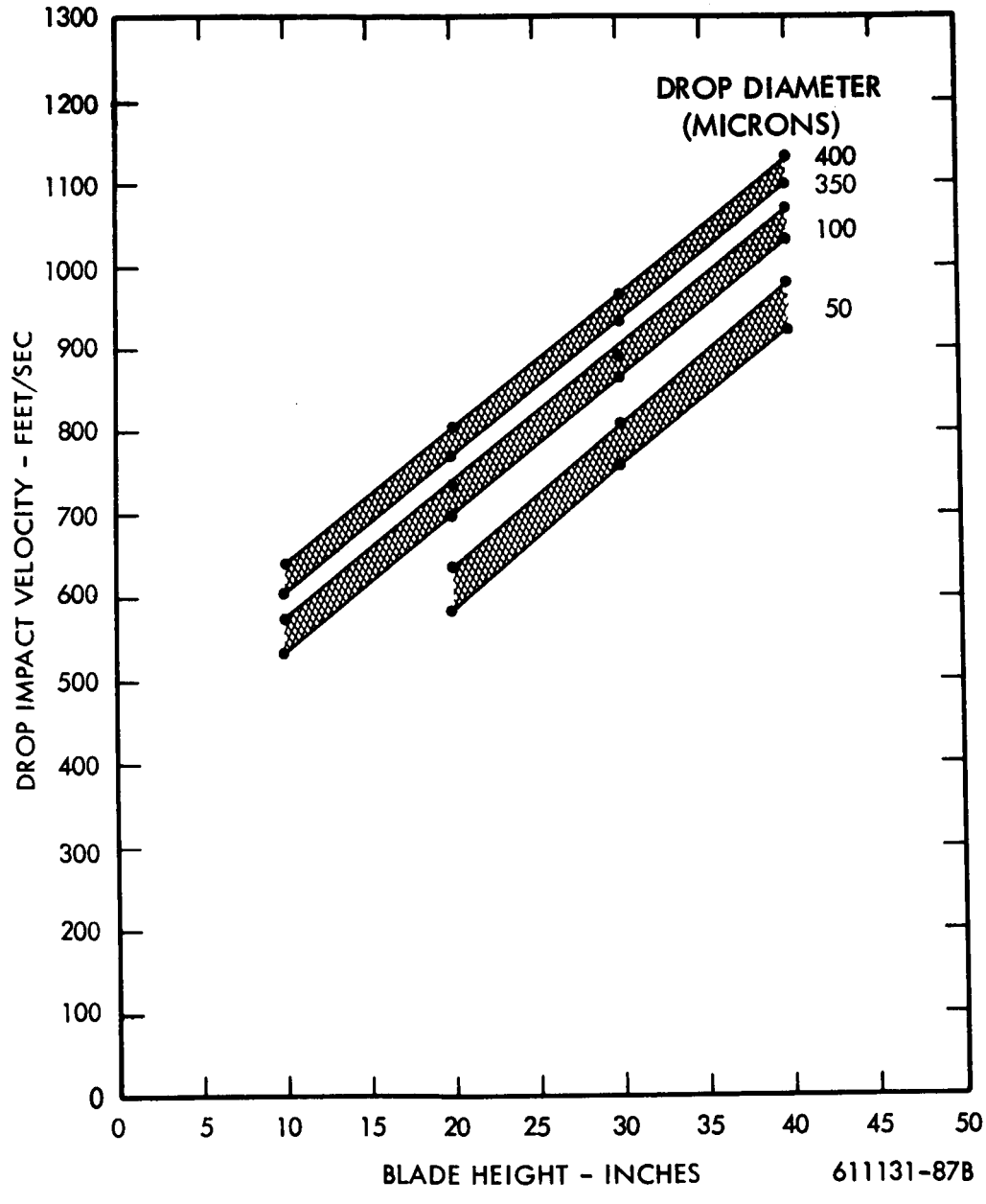

Figure B-20. Yankee Turbine Ninth Rotor Drop Impact Velocities

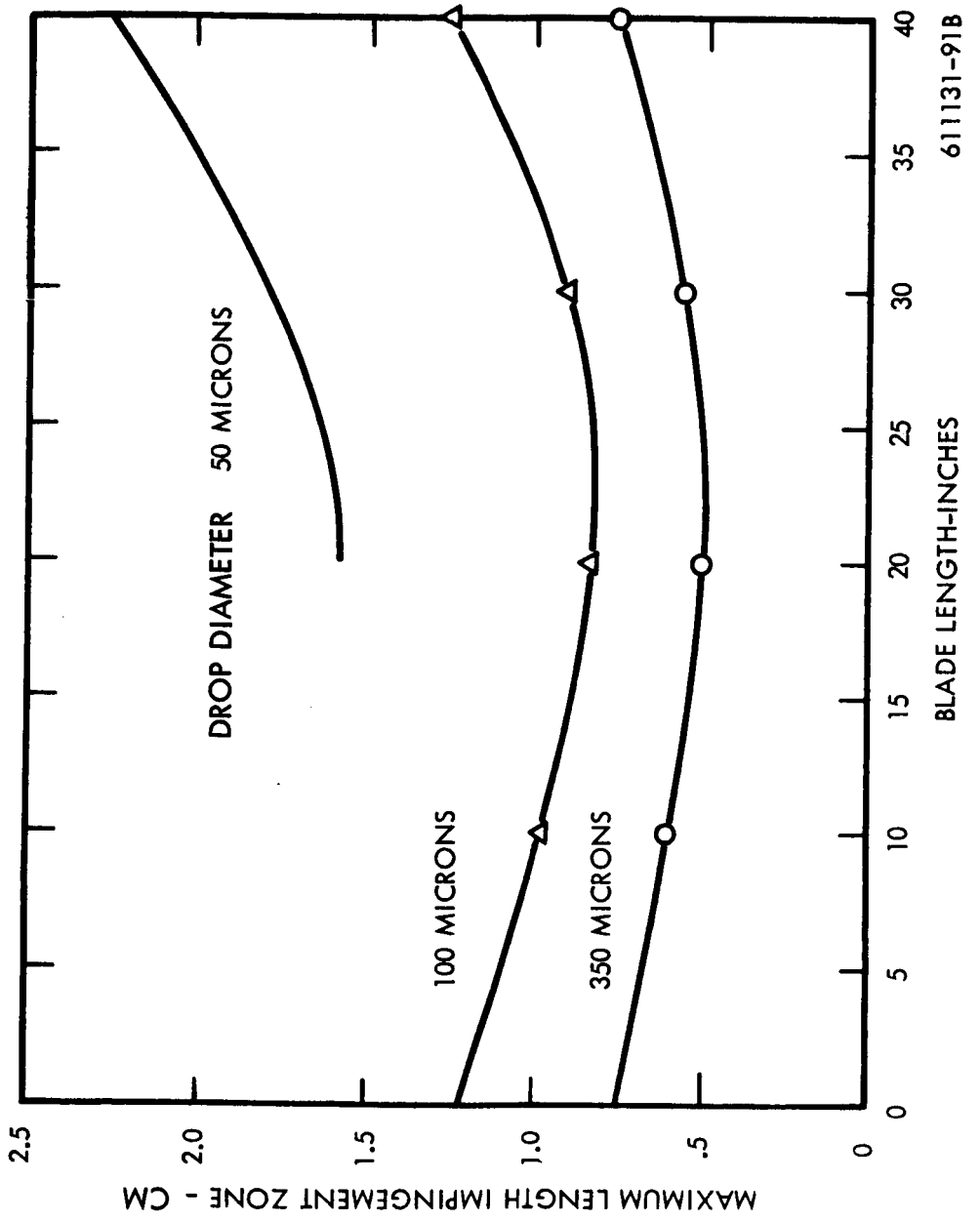

Figure B-21. Axial Length Impingement Zone (Maximum)

impacting the rotor of an actual English steam turbine[27]. Also, the range of drop sizes seen departing from stators, reported by CERL [25] and Rocketdyne Division of North American Aviation[24] (Contract NAS 7-391), appears similar to those calculated here. However, to obtain an adequate check on this or any model of atomization, acceleration, and impingement of damaging moisture, requires more extensive and complete sampling of the total spray produced under turbine-like conditions than has been done to date. The reported experimental work thus far has involved selective examination of a few drop trajectories and atomization processes, rather than a comprehensive summation in numerical terms that describe the total spray. Such a total summation is required for erosion calculations.

In conclusion, the proposed model of damaging liquid history from stator to rotor bears a substantial resemblance to reality in spite of numerous simplifications and assumptions. The quantitative degree of validity of the model cannot be determined from the reported experimental data available. It is recommended that experiments be conducted to provide numerical values of the total characteristics of turbine sprays rather than the selective observations performed to date.

3.6 Material Removal

The approach taken to obtain quantitative values of material removal rates, with respect to physical impact and chemical effects is essentially empirical. Observed rates, as reported in the literature, have been empirically correlated in terms of gross external variables. These correlations are then applied to turbine conditions to yield numerical values of erosion.

Obviously, such an approach is reasonable only if the data has been taken under conditions similar to the application or if the calculational method can be checked against such data. A small amount of such data has become available recently. The data on removal by repeated drop impingement are those of Pearson[28] of the CEGBof Great Britain. Information on chemical removal in flowing liquid metal systems has been reported by ORNL[29].

Chemical Effects

In the early days of steam turbines it was postulated that chemical effects might play a part in the observed blade erosion. While the presence of such effects has never been conclusively disproved, there seems to be no body of opinion that considers them to be of any

importance. The observed erosion in steam turbines can be adequately explained as a physical phenomenon without recourse to chemical explanations. The pure physical model is that applied to the steam turbine.

The chemical situation in respect to liquid metals is not as clear. Because of the elevated operating temperatures and the nature of the fluids involved in liquid metal turbine systems all proposed structural materials have a substantial degree of solubility in the working fluid. In pure fluid systems,such as can be maintained with reasonable "state of the art" technology with liquid metal working fluids, it is felt that dissolution of the blade materials is the main chemical possibility for material removal and that quantitative data generated today can be extrapolated to other similar systems for rough, predictive comparisons.

In a wet vapor turbine the greatest concentration of liquid on the blades would be along the convex side of the rotor blades near the nose where most of the collected moisture from the stators impinges. The impinging moisture will then flow almost radially outward along the face of the blade until discharged at the tip. This provides a steady-flow process where liquid is continually supplied and removed for dissolution of blade materials, without allowing the working fluid to come to saturation.

According to Epstein[30], the dissolution of a metal into a liquid can be described as:

$$n(t) = n_o \left[1 - \exp\left(-k \frac{A}{V} t\right)\right]$$

where:
- $n(t)$ = concentration of dissolving solute as a function of time
- n_o = equilibrium saturation solubility of solute in the solvent
- A = area of contact between solid and liquid
- V = volume of liquid in contact with the solid
- t = time of contact
- k = solution-rate constant

The parameter k varies with temperature, flow rate (mixing), materials, surface, etc. and must be determined for each system under consideration. Although few k values are recorded in the literature, the values and systems in table B-10 indicate the range of k. The value, $k = 5 \times 10^{-6}$ cm/sec, was selected for calculational purposes here, and is based on the information in reference 32. The system reported therein is an alkali metal system.

TABLE B-10

Solution-Rate Constants

System	Temperature (°C)	k (cm/sec)	Reference
Cu → Pb (liq.)	510	6.07×10^{-4}	31
Cu → Bi (liq.)	510	1.91×10^{-3}	31
304 s/s → Li (liq.)	510	1.54×10^{-6}	32
304 s/s → Li (liq.)	612	7.50×10^{-6}	32

Additional inputs required to solve the Epstein equations are the saturation solubilities of the various structural material components and the liquid flow rates. A sample calculation is given in Part C of Volume III. By use of a representative liquid flow rate and by assuming that the constituents most seriously attacked were iron-like, a rate of material removal of 2.3 mils/10,000 hours of exposure was obtained.

ORNL[29], reporting on attack by flowing (NaK (2-10 ft/sec) in the SNAP-8 system, found that maximum attack occurred in a system (with less than 30 ppm oxygen) on Hastalloy N at the outlet end of the SNAP-8 reactor. Extrapolation of this data indicates that corrosion at this point will be less than 1.5 mils in 10,000 hours at 1300°F. These figures indicate the relative range of dissolution attack by direct chemical action that could be expected in a system of low oxygen concentration at low flow velocities. Unless flow rates* across turbine blades are substantially higher than those of the sample calculation, it would seem unlikely that direct chemical dissolution will result in any serious damage by alkali metals to turbine rotor blades.

It is known that chemical dissolution of a material into a liquid metal occurs preferentially on the least densely packed crystal surfaces and at grain boundaries. Such preferred dissolution may have a weakening effect on the material which, when coupled with the impact stresses of droplets, may result in accelerating the impact erosion process. At present

* If as suggested by Epstein, $k \sim \bar{v}^{0.8}$ (where $\bar{v}$ is the liquid velocity), then Epstein's equation would be relatively insensitive to the effect of velocity at a constant volumetric flow. The product kt being $\sim \frac{1}{V^{0.2}}$. This would imply that it is unnecessary to account, as to dissolution, for the very high momentary flow velocities that exist at drop-surface impact and is the implied assumption used here.

there is insufficient data to support or refute this hypothesis with respect to liquid metal working fluids.

Physical Removal by Liquid Impingement

Some simple correlations of the erosion rate of steam turbine materials are presented as a function of repetitive water drop impacts. The original data, by Pearson [28], is suitably arranged to allow predictions of Yankee steam turbine erosion rates as a function of calculated impacts. No attempt has been made to correlate similar data for candidate liquid metal turbine blade materials. The information in the literature is inadequately reported and does not appear to supply meaningful quantities in terms of calculated impaction on turbine blades. Fortunately, the amount of damaging liquid which collects in the two-stage potassium turbine is so small that this latter step seems unnecessary.

These correlations are the result of an examination of the available literature on removal of material from steam turbine blade materials by water drop impact. This study is reported in depth in Volume III, Part A. During this examination the possible number of independent variables was reduced from eleven or twelve to three which are the most important*. These are (1) velocity of impact, (2) angle of impact and (3) impacting drop size.

As pointed out in Volume III, one of the greatest difficulties in interpreting and correlating erosion test data is not the multiplicity of the independent variables, but the identification of the dependent variable(s) for characterizing erosion. All would be well if, under given conditions, erosion proceeded at a constant rate and could be unmistakably characterized by a uniform slope of a cumulative weight loss versus time curve. Since erosion rates are not constant with time, erosion can be only approximately characterized by a simplified time independent approach.

The most accepted view is that the first stage in erosion shows little or no weight loss and represents plastic deformation of the surface and initiation of fatigue cracks. This stage merges into the second stage in which the rate of weight loss is at a maximum and approximately uniform over a period of time. This, in turn, merges into a later stage (or stages) in which the erosion rate diminishes and may or may not tend toward another uniform value. Whatever the precise cause of this decrease in erosion rate may be, it is usually associated with rather

* For a given impacting fluid and impacted material pair.

general and severe damage to the surface, which through geometrical effects alone may result in an effective alteration of the impingement conditions.

It is assumed that the uniform rate of the second stage is the most meaningful in predicting the total erosion in the steam turbine. This assumes that the bulk of the erosion of the blades takes place during this second stage. The time period of the first stage is short compared with the total operating time. Turbine designs which demonstrate severe enough erosion rates in the second stage to become third stage terminal cases will suffer from a lack of customer interest and disappear. In any case, from a design point of view, using a second stage rate is a conservative assumption.

Pearson has measured the erosion from samples of Stellite 6 and 6B* subject to multiple impacts of water of controlled size, direction and speed, and has correlated the data using second stage of erosion rates for these Stellites and other steam turbine materials in the form:

$$\frac{\Delta W_m}{\Delta W_w} = k (V_n - V_{cd})^n \sec \theta$$

where: $\frac{\Delta W_m}{\Delta W_w}$ is the mass of material removed per unit mass of impinging water

V_n is the component normal to the impacted surface of velocity of impact

V_{cd} is a critical or threshold velocity below which erosion is negligible

θ is the angle between the impact velocity vector and the normal to the surface

k, n are empirical constants

Data from Pearson for Stellite 6 and 6B are plotted in figure B-22. The sec θ correction is ignored because the angles of impact at which the data were taken were always within 30 degrees of the normal to the surface. The correlation of figure B-22 thus gives "the erosion" in terms of two out of three of the independent variables of primary importance.

---

* Stellite 6B is the erosion shield material used on the Yankee turbine rotor blades.

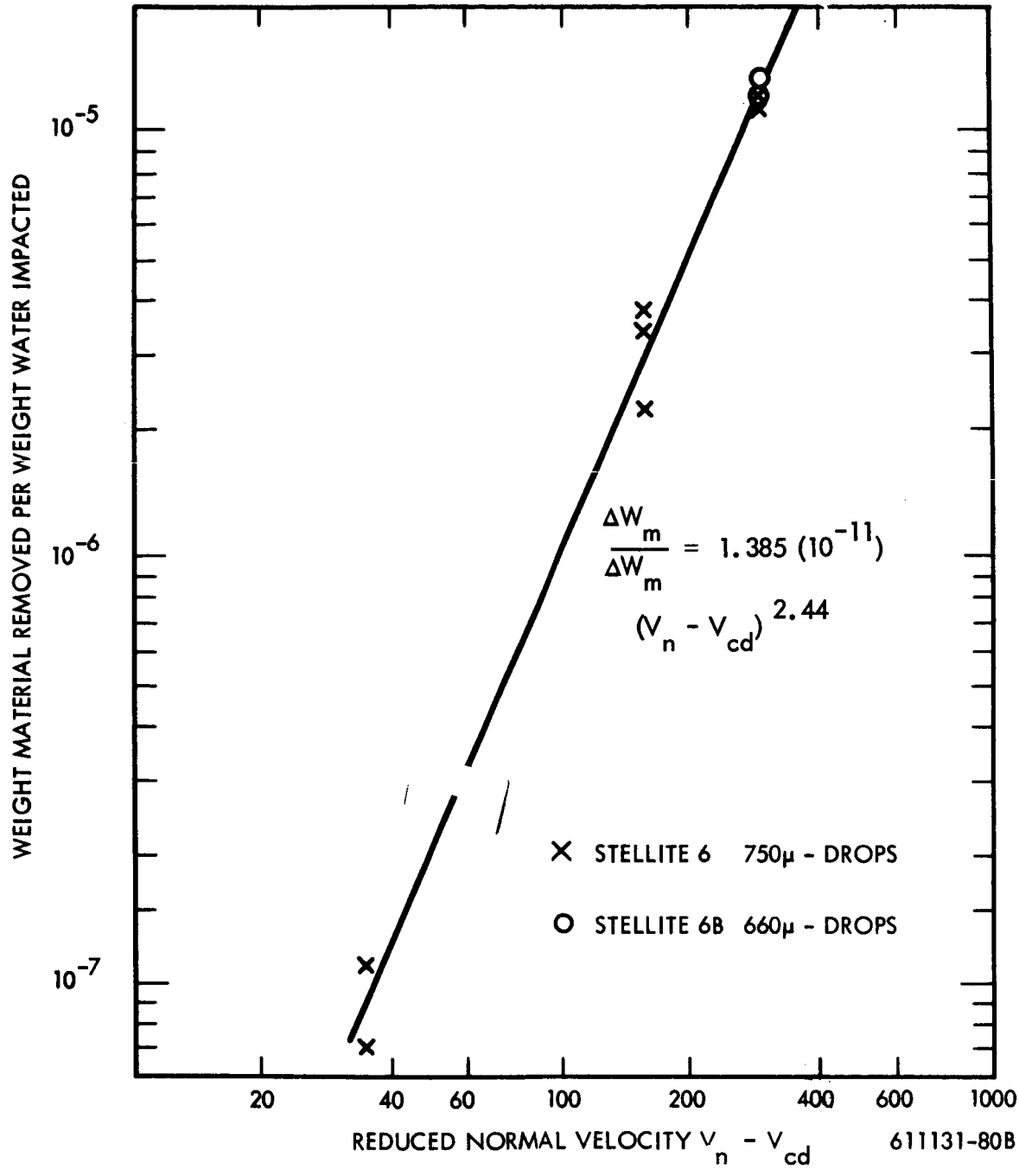

Figure B-22. Stellite Erosion Rates - Data from Pearson; Reduced Normal Velocity ($V_n - V_{cd}$)

A correlation for the third independent variable, drop size, was also derived from Pearson's data. This correlation uses the observation that the threshold velocity of normal impact below which erosion is negligible appears to be a regular function of drop size. Assuming that:

$$V_{cd} \propto \sqrt{\frac{1}{D}} ,$$

where D is the diameter of the impinging drops. As shown in figure B-23, the correlations are quite good.

The data of figure B-23 was taken using a stainless steel. Since there was insufficient spread to attempt a similar correlation in drop sizes in the data reported for the Stellites, it was assumed that the form for the Stellites would be approximately the same as for stainless steel with a different empirical constant relating the proportionality between V_{cd} and $D^{-1/2}$. This yielded the expression:

$$V_{cd} = \sqrt{1155/D} \quad .$$

where D = drop diameter, ft

V_{cd} = threshold velocity, ft/sec

The foregoing expression used in conjunction with figure B-22 is then arithmetically sufficient to calculate material removal rates for Stellite 6B, if the states of the impacting fluid are known.

4.0 CALCULATED EROSION RATES

4.1 Yankee Turbine

Once numerical values are established in a turbine for the overall flow conditions and the detail processes leading to erosion, the erosion rate can of course be calculated. In the calculations, for which the results are presented hereafter, a simplifying assumption was made. This assumption is that the liquid impinging in the drops sufficiently large to cause erosion damage, is uniformly distributed over these size classes. This assumption underestimates the proportion of liquid in the heavier drop size classes, but the simplification appears warranted on the basis that the erosion calculation is more sensitive to other parameters. Using

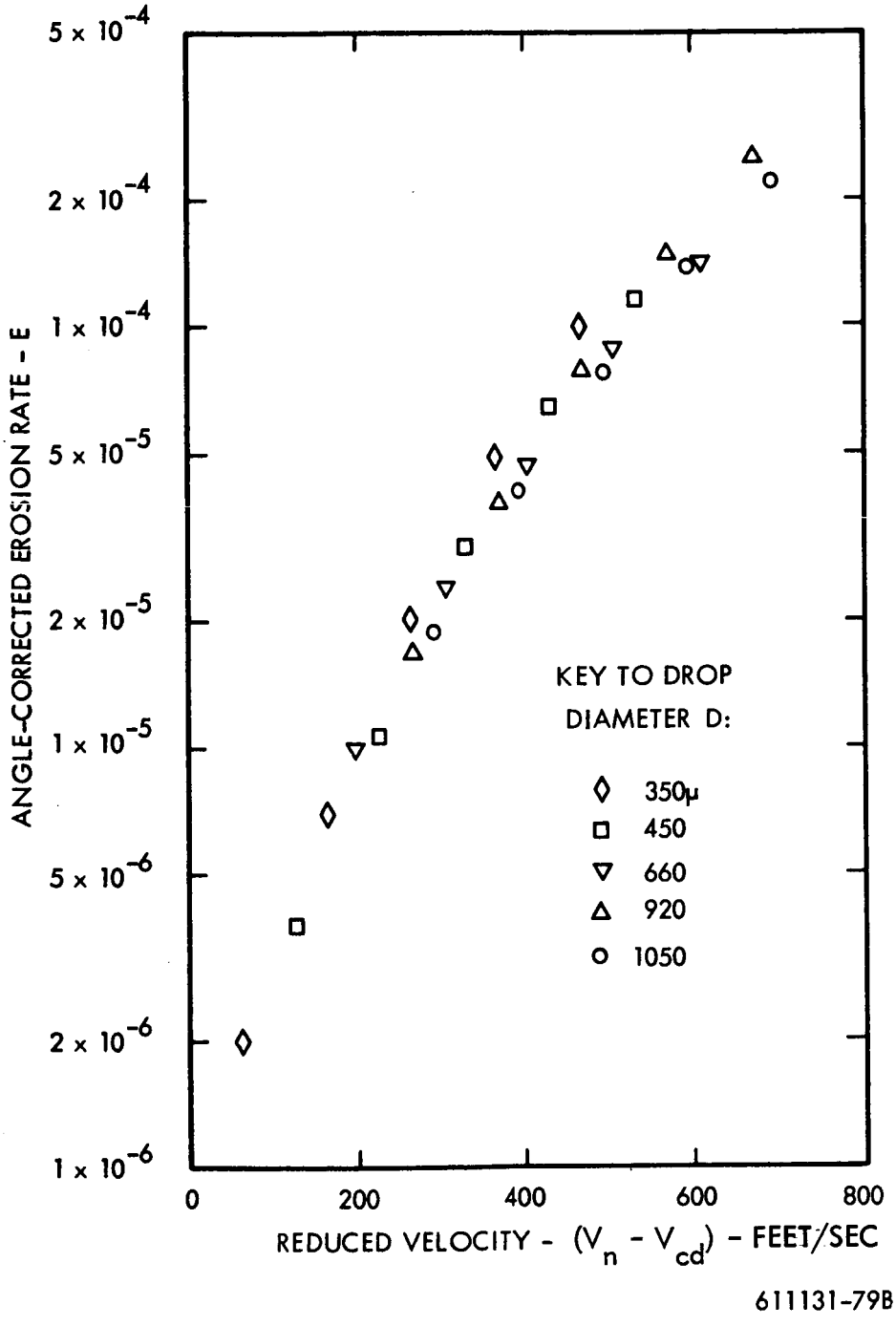

Figure B-23. Correlation of Data of Pearson by use of "Critical Velocity"

this assumption (for a turbine material having a characteristic slope of material removal versus reduced normal velocity as shown in figure B-22) that the average erosion per unit of water impacted is given by a velocity difference $(V_n - V_{cd})$ which is 61 percent of the maximum velocity difference (the heaviest, slowest drop velocity difference) encountered.

$$W_m = 1.385\,(10^{-11}) \int_{V_n = V_{cd}}^{V_{n(max)}} (V_n - V_{cd})^{2.44}\, d(W_w); \text{assumption } (W_w) = K\,(V_n - V_{cd})$$

Substituting for $d(W_w) = Kd\,(V_n - V_{cd})$ and integrating the first expression gives

$$W_m = 4.02\ (10^{-12})\,(V_{n_{(max)}} - V_{cd})^{3.44}\ (K)$$

or

$$\frac{W_m}{W_w} = 4.02\,(10^{-12})\,(V_{n_{(max)}} - V_{cd})^{2.44}$$

Define

$$\frac{W_m}{W_w} = 1.385\,(10^{-11})\,(\overline{V}_n - V_{cd})^{2.44}$$

then

$$4.02\,(10^{-12})\,(V_{n_{(max)}} - V_{cd})^{2.44} = 1.385\,(10^{-11})\,(\overline{V}_n - V_{cd})^{2.44}$$

or

$$\frac{(\overline{V}_n - V_{cd})}{(V_{n_{(max)}} - V_{cd})} = 0.61$$

where

$V_{n_{(max)}}$ = maximum velocity of a class of drops relative to the rotor blade

$\overline{V}_n$ = average effective velocity of a class of drops relative to the rotor blade

The following numerical values are for the ninth stage of the Yankee turbine:

1	Flow (Steam plus water)	801,100 lb/hr	(Table B-2)
2	Average Percent Moisture Ninth Stator	13.5 %	(Table B-2)
3	Average Fog Particle Size (η_p = 85%)	0.44 μ radius	(Table B-5)
4	Portion Collected Ninth Stator, Nose	~ 1 %	(Figure B-12)
5	Portion Collected Ninth Stator, Concave Surface	~ 1.5 %	(Figure B-14)
6	Portion Collected Ninth Stator, Total	~ 2.5 %	
7	Total Moisture Impacting Ninth Rotor	1230 kg/hr	
8	Number Blades Ninth Rotor	196	(Section 2.1)
9	Length of a Ninth Rotor Blade	101.5 cm	(Table B-2)
10	Total Length Ninth Rotor Blades	1.99 (10^4) cm	
11	Average Rate of Moisture Impact	62 gm/cm/hr	
12	Total Moisture Impacted in 13,000 hrs.	803 kg/cm	(~ 1 ton)

Assuming the moisture is uniformly distributed from hub to tip on a time average basis, then item 11, previously given, is the overall local rate per unit of blade length. The damaging portion of this moisture is that contained in all drops of greater than damaging size. The minimum damaging size at any particular blade length is that size which impacts with the critical velocity as given by:

$$V_{cd} = \sqrt{\frac{1155}{D}}$$

The calculated velocities of impact to be matched to the critical velocities of impact to determine the critical size are taken from figure B-20, (Ninth Yankee Rotor Drop Impact

Velocities). The percentage of the total moisture in the form of damaging sizes can be then determined from figure B-17 if the maximum size drop impacting is selected. This information may in turn be converted into damaging liquid rates per unit of area per unit of time by use of information similar to that in figure B-21. The results of such calculations are shown in the third column of tables B-11 and B-12. This information is then used in conjunction with further reference to figure B-20 to obtain the maximum drop impact velocity and by reference to figure B-22, to complete the erosion calculation for which values are given in the remaining columns of tables B-11 and B-12.

4.2 Discussion of Results

In the actual Yankee turbine, at the time of the 1962 shutdown, after the first 18 months of operation, there was evidence of erosion on the leading edge of the rotor blades in the last blade row (ninth) of the low pressure turbines. Erosion in both turbines was very nearly the same. While the intensity of the erosion varied throughout the ninth row the erosion position was roughly the same, extending an approximate distance of 2 inches in from the tip of the blade with maximum intensity approximately 3/4 inches from the tip. The depth of erosion varied from a maximum of 62 mils to 190 mils (about 8 blades of 196) to a minimum of no more than roughening of the inlet edge.

The calculated results as given in tables B-11 and B-12 correctly predict that any appreciable erosion would be confined to the outer portion of the blades. They incorrectly predict that the maximum erosion would occur at the very tip of the blade instead of 3/4 inches in from the tip as actually observed. The two average calculated values of maximum depth of erosion, 3 mils, table B-11, 15 mils, table B-12, are certainly of the right order of magnitude since the reported depths varied from essentially 0 to 180 mils.

It would appear that the values calculated using the suction side wake calculation for maximum stable primary drops gives the more reasonable average maximum erosion in terms of the overall spread of the reported depths of erosion. However, it would be misleading to conclude that

TABLE B-11

Calculated Erosion Ninth Rotor Yankee Turbine
Maximum Stable Drop Size Criterion - W_e = 22, Pressure Side Wake

Drop Size Interval (microns)	Blade Length from Hub (inches)	Average Liquid Rate of Impact ($gm/cm^2/hr$)	61 Percent $(V_n - V_{cd})$ Max (ft/sec)	Erosion Rate ($gm/cm^2/hr$)	Average Erosion in 13,000 hrs (gm/cm^2)	Average Depth Erosion in 13,000 hrs (mils)
350 - 275	40	6.4	80	$0.45\ (10^{-5})$	0.059	2.8
350 - 300	38	5.1	60	$0.17\ (10^{-5})$	0.022	1.0
350 - 320	36	3.8	43	$0.05\ (10^{-5})$	0.004	0.2

TABLE B-12

Calculated Erosion Ninth Rotor Yankee Turbine
Maximum Stable Drop Size Criterion - W_e = 22, Suction Side Wake

Drop Size Interval (microns)	Blade Length from Hub (inches)	Average Liquid Rate of Impact ($gm/cm^2/hr$)	61 Percent $(V_n - V_{cd})$ Max. (ft/sec)	Erosion Rate ($gm/cm^2/hr$)	Average Erosion in 13,000 hrs (gm/cm^2)	Average Depth Erosion in 13,000 hrs (mils)
400 - 275	40	14.0	120	$2.5\ (10^{-5})$	0.33	15.5
400 - 300	38	13.0	102	$1.4\ (10^{-5})$	0.18	8.6
400 - 320	36	12.3	83	$0.9\ (10^{-5})$	0.12	5.5

the damaging moisture originated on the suction side. While no error analysis of the calculations was carried out, it is unlikely that the calculated Weber No. for any particular drop is sufficiently accurate to allow this observation to be made.

Implicit in this final summary erosion calculation is the observation that only the large primary drops detached from the stators which do not undergo a secondary breakup cause erosion damage. This study differs from all previous analytical studies in accounting for these residual drops. It also is the first study to our knowledge which is carried to the logical conclusion of calculating erosion rates. Previous studies carried to this end, as they do not account for the residual primary drops, would have been forced to conclude that erosion did not take place in steam turbines.

In previous Westinghouse internal qualitative explanations of the observed erosion patterns at the tips of the rotor blades it has been usual to postulate concentration of the collected liquid to the periphery of the turbines as well as velocity vector effects. On the basis of this quantitative evaluation it appears that the velocity vector effects are sufficient in themselves to largely explain observed patterns. The effects of concentration appear to be relatively unimportant.

As has been shown by the comparisons afforded in calculated erosion rate by tables B-11, B-12, the erosion level in the Yankee turbine is near a threshold. The erosion rate at the threshold is most sensitive to the maximum drop size impinging upon the rotor blades and hence to the criteria used to determine the maximum drop size.

While not explicitly shown in the calculations in Section B4.1, another area of calculational sensitivity is concerned with the total amount of liquid collected by a stator. As can be seen from figures B-11, B-12, and B-14, the amount collected is quite sensitive to fog particle size in the calculated diameter range (0.87μ). The size of fog particle in turn is quite sensitive to the surface tension of the liquid and the expansion rate when nucleation is occurring. This was discussed in Section B3.1.

Considering the sensitivity of the overall erosion rate calculation to relatively small changes in numerical values of some of the component processes, the agreement between calculated and observed values is good.

4.3 Two-Stage Potassium Turbine

An arithematic calculation similar to that for the steam turbine was carried out for the potassium turbine except that the calculation was terminated short of a complete numerical depth of erosion determination. This was done because it was discovered that the calculated amount of moisture collected was much less than for the steam turbine. This coupled with a much shorter total period of operation for the potassium test turbine as compared to the steam turbine led to the conclusion that not much(if any)erosion would be shown by such a calculation.

The following numerical values are for the second stage of the potassium turbine:

1	Flow (vapor plus liquid)	2.64 lb/sec	Subsection B2.2
2	Average Percent Moisture, Second Stator	4.4 %	Table B-6
3	Average Fog Particle Size	0.12 μ radius	Subsection B3.1
4	Portion Collected, Second Stator Nose	~0 %	Figure B-13
5	Portion Collected, Second Stator Concave Surface	~0.3%	Figure B-15
6	Portion Collected, Second Stator Total	~0.3%	
7	Total Moisture Impacting, Second Rotor	0.55 kg/hr	
8	Number Blades, Second Rotor	60	Subsection B2.2
9	Length of a Second Rotor Blade	2.5 cm	Table B-3
10	Total Length, Second Rotor Blades	150cm	
11	Average Rate of Moisture Impact	3.6gm/cm/hr	
12	Total Moisture in 2000 hours	7.2kg/cm	

Compare the value of item 12, 7.2 kg/cm, (the total amount impacted per unit of rotor blade length in 2000 hours) against the corresponding value of 803 kg/cm from the steam turbine in

13,000 hours. This reveals that the amount of calculated total moisture impacting the potassium turbine is almost a factor of 112 less than for the steam turbine. As mentioned previously, it therefore seemed unnecessary to complete the calculations to obtain an estimate of negligible erosion* unless this amount of collected liquid will cause appreciable chemical dissolution of the blading material. As discussed in Section B3.6, this later event seems unlikely.

---

* This is, of course, only true if the physical situation is not a factor of 10^2 worse in the potassium turbine as compared to the steam turbine. In general terms this breaks down into the erosion resistance of the potassium turbine blade materials to impact erosion, the size of the drops impacting, and the severity of impact which will be assumed proportional to the Waterhammer expression, ρcv.

ρ - liquid density
c - liquid acoustic velocity
v - normal velocity of impact

Material Resistance

One of the principal blade materials used in the two-stage potassium test turbine was Udimet 700. This alloy is of the same family as René 41 (Udimet 41+). Young and Johnston[34] have compared second stage erosion loss rates under cavitating conditions in sodium at 800°F of René 41 and Stellite 6B. They found the following: (by our manipulation of their data)

Stellite 6B -- 4. (10^{-5}) gm/cm^2/hr
René 41 -- 11. (10^{-5}) gm/cm^2/hr

Note the Stellite 6B rate is similar to that found for the Yankee turbine.

Drop Size

A Weber No. criterion for maximum drop size was used in the Yankee calculations. This was a local Weber No. in the wake. However, to a first approximation this Weber No. should be proportional to the bulk flow Weber No.

By this reasoning, the relative size of drops between the potassium turbine and the steam turbine should be given (to a first approximation) by the ratio of the quantity

$$\frac{\sigma}{\rho_o U_o^2}$$

where σ is the liquid surface tension
ρ_o is the vapor bulk density
U_o is the vapor bulk velocity

Stator Exit	$\frac{\sigma}{\rho_o U_o^2}$
Yankee 9th	$2.8\ (10^{-5})$ ft
Potassium 2nd	$3.7\ (10^{-6})$ ft

Impact Severity

Since the maximum velocity of impact of drops on the potassium turbine has not been calculated, it will be assumed that it corresponds to the worst possible case. That is, the velocity of impact is equal to the tip speed of the second rotor blades.

Rotor	ρcV
Yankee 9th	$10.3(10^6)$ lb/ft^2
Potassium 2nd	$5.2\ (10^6)$ lb/ft^2

The conclusion drawn from this comparison is that the physical erosion picture for the potassium turbine is at least as favorable as that in the steam turbine, disregarding the relative amounts of moisture present.

PART C

CONCLUSIONS AND RECOMMENDATIONS

A continuous analytical model of rotor blade erosion in wet vapor turbines has been constructed in sufficient detail to allow calculations of numerical values of depth of erosion. The model has been used to examine the erosion of two wet vapor turbines on which there is experimental information. The turbines investigated are analytical simulations of: (1) the low pressure steam turbine of the Yankee Atomic Plant and (2) the General Electric two-stage potassium test turbine of Contract NAS5-1143.

With some reservation, the estimated erosion can be considered to be in agreement with observed erosion. The overall model selected appears to be adequate for at least order of magnitude turbine erosion estimation and provides an excellent basis for further refinement.

To improve and refine the model both analytical and experimental effort is recommended. Major analytical efforts should be directed at the theoretical deficiencies and uncertainties which are present in the condensation and condensate collection models as now formulated. In particular in the condensation area (1) the effects of association of molecular species in liquid metal vapors and (2) the possible effects of condensed moisture carried over into the turbine inlet from upstream equipment should be thoroughly examined. In the condensate collection area a thorough search for information on very fine particle separation should be made in conjunction with continued analytical examination of the possible mechanisms of such separation.

Major experimental efforts should be directed, at this time, to the areas of condensation, atomization from stators, and material removal by liquid drop impact. In particular, spontaneous condensation experiments should be run in wet vapors in which condensate particle size is accurately measured in addition to the usual thermodynamic and flow quantities. Experiments with the liquid metals are particularly desirable.

Experiments in atomization of liquids under the impress of passing gas or vapor streams from stator-like trailing edges should be conducted. These experiments should be aimed at characterizing the total sprays so produced rather than on an examination of the detail processes as such.

A great deal more experimental information on material removal rates by liquid drop impact should be obtained under widely varying, carefully controlled and accurately reported velocities, angles of impingement, and drop sizes for selected candidate turbine blade materials and probable companion working fluids. These investigations should be more oriented toward obtaining empirical engineering information of quantitative use to the turbine designer, rather than to a fundamental understanding of the extremely complex material removal processes.* Due regard in these experiments must be paid to the "past history influence" on any particular reported erosion rate. (The "state"** of the surface eroded at the time of measurement).

---

* It seems unlikely to this writer that a quantitative theory of material removal by liquid drop impact (a transient process) can be constructed prior to the existence of a complete quantitative theory explaining steady state behavior of structural materials.

** "State" is meant to convey a characterization of both a surface damage condition and a stage of erosion .

REFERENCES

1. Gyarmathy, G., The Bases for a Theory of the Wet Steam Turbine, Juris-Verlag, Zurich, 1962.

2. Gardner, G. C.,"Events Leading to Erosion in the Steam Turbine," Proc. Inst. Mech. Engrs., 178, Pt 1, No. 23, pp 593 to 623, 1963-1964.

3. Schnetzer, E., Two Stage Potassium Test Turbine, Quarterly Progress Report No. 18, August 8, 1965 through November 8, 1965, NASA Contract NAS 5-1143, Jan. 10, 1966

4. Schnetzer, E., Two Stage Potassium Test Turbine Quarterly Progress Report No. 15. (Nov. 8, 1964 - Feb. 8, 1965), Missile and Space Division, General Electric Company, NASA Contract NAS 5-1143.

5. Rossbach, R. J., Space-Vehicle Rankine-Cycle Power Plant, Potassium-Turbine Development, Space Power and Propulsion Section, General Electric Company, ASME Paper 63-WA-326.

6. Joyce, J. P., Contract NAS 5-1143, Two-Stage Potassium Vapor Turbine, NASA Lewis Research Center, Nuclear Power Technology Branch, Letter 9212, March 15, 1966.

7. Stever, H. G., Condensation Phenomena in High-Speed Flows, Fundamentals of Gas Dynamics, Princeton University Press, 1958.

8. Courtney, W. G.,"Recent Advances in Condensation and Evaporation," ARS Jour., 31, pp 751 to 756, June 1961.

9. Oswatitish, K. Z., Ver. dent Ing., 86, p 702, 1942.

10. Glassman, A. J., Analytical Study of the Expansion and Condensation Behavior of Alkali-Metal and Mercury Vapors Flowing Through Nozzles, NASA-TND-2475, Sept. 1964.

11. Hill, P. G., H. Witing, and E. P. Demetri,"Condensation of Metal Vapors during Rapid Expansion," Trans. ASME (Heat Transfer), Vol. 85, Part C.

12. Gyarmathy, G., and Meyer, The Bases for a Theory of the Wet Steam Turbine, Juris-Verlag, Zurich, 1962.

13. Frenkel, J., Kinetic Theory of Liquids (Oxford) pp 366 to 426.

14. Kantrowitz, A.," Nucleation in Very Rapid Vapor Expansions," J. Chem. Phys., Vol. 19, No. 9, pp. 1097 to 1100, September 1951.

15. Frisch, H. L. and C. Willis, "The Kinetics of Phase Transitions Involving Dimer Reactions," J. Chem. Phys., 22 No. 2, pp. 243 and 244, February 1954.

16. Katz, J. L., H. Saltsburg, and H. Reiss, Nucleation in Associated Vapors, North American Aviation Science Center, SCPP-65-32, May 18, 1965.

17. Goldman, L. J. and S. M. Nosek, Experimental Determination of Expansion and Flow Characteristics of Potassium Vapor Through a Nozzle, Unpublished as of October 1, 1965.

18. Truckenbrodt, E., A Method of Quadrature for Calculations on the Lominar Boundary Layer in Case of Plane and Rotationally Symmetrical Flow, NACA-TM-1379, May 1955.

19. Preston, J. H., "The Minimum Reynolds No. for a Turbulent Boundary Layer and the Selection of a Transition Device," Journ. of Fluid Mech., Vol. 3, p. 373, 1957-1958.

20. Lieblein, S., and W. H. Roudebush, Low-Speed Wake Characteristics of Two-Dimensional Cascade and Isolated Airfoil Sections, NACA-TN-3771, October 1956.

21. Heskestad, G., and D. R. Olbertz, "Influence of Trailing-Edge Geometry on Hydraulic-Turbine-Blade Vibration Resulting from Vortex Excitation," Trans. ASME-Jo. Eng. Power, p. 103, April 1960.

22. Brun, R. J., W. Lewis, P. J. Perkins, and J. S. Serafini, Impingement of Cloud Droplets on a Cylinder and Procedure for Measuring Liquid-Water Content and Droplet Sizes in Supercooled Clouds by Rotating Multicylinder Method, NACA Report 1215, 1955.

23. Emmons, H. W., Fundamentals of Gas Dynamics, Vol. III, Sec. H., Princeton, Princeton University Press, 1958.

24. Degner, V. R., Quarterly Status Letter No. 3, Contract NAS 7-391, Investigation of Variables in Turbine Erosion, North American Aviation Inc., Rocketdyne Division, 66RC5335.

25. Hays, L. G., Turbine Erosion Research in Great Britain, NASA, Jet Propulsion Lab. C.I.T. Tech. Memo No. 33-271.

26. Wolfe, H. E., and W. H. Andersen, Kinetics, Mechanism, and Resultant Droplet Sizes of the Aerodynamic Breakup of Liquids, Aerojet-General Corp., Report 0395-04-18SP, April 1964.

27. Christie, D. G., G. W. Hayward, Observations of Events Leading to the Formation of Water Droplets which Cause Turbine Blade Erosion, Meeting of the British Royal Society, May 27, 1965.

28a. Pearson, D., A Summary of the M.E.L. Experimental Data on Erosion, C.E.G.B., RID. Dept. (Gr. Brit.), Marchwood Engrg. Labs, RDD/M/M18, Job. No. 30023, November 1964.

28b. Pearson, D., The Effect of Drop Size on the Erosion of a Stainless Steel Central Electricity Generating Board (Great Britain), Report RD/M/N128, December 1964.

29. ORNL-3898, SNAP-8 Corrosion Program, Summary Report, December 1965.

30. Epstein, L. F., Static and Dynamic Corrosion and Mass Transfer in Liquid Metal Systems, Chem. Eng. Prog. Symp. Series, Vol. 53, No. 20, p. 67, 1957.

31. Ward, A. G., and J. W. Taylor, "Solution-Rate Studies with Liquid Metals: Solution of Copper in Liquid Lead and Bismuth," Journal of Inst. of Metals, Vol. 85, p. 145, 1956-1957.

32. Gill, W. N., et al, "Mass Transfer in Liquid-Lithium Systems," A.I.Ch.E. Journal, Vol. 6, No. 1, p. 139, 1960.

33. Nukiyana, S., Y. Tanasana, as quoted in A. A. Putnam, et al, Injection and Combustion of Liquid Fuels, Battelle Memorial Institute, WADC Technical Report 56-344, May 1957.

34. Young, S. G., J. R. Johnston, Accelerated Cavitation Damage of Steels and Superalloys in Sodium and Mercury, Paper No. 121, 69th Annual Meeting of the ASTM, Atlantic City, N. J., June 27 - July 1, 1966.

35. Goldman, L. J., S. M. Nosek, Experimental Determination of the Expansion and Flow Characteristics of Potassium Vapor Through a Nozzle, NASA - Lewis Laboratory, 1965.

36. Cohen, E., STL Heavy Particle Propulsion Program P.2, Third Symposium on Advanced Propulsion Concepts, OSR, USAF, and G.E. Co., Cincinnati, Ohio, October 2-4, 1962.

37. Space Power Systems, Advanced Technology Conference, Lewis Research Center, Cleveland, Ohio, August 23, 24, 1966, NASA.